https://doi.org/10.5194/tc-2020-53
Preprint. Discussion started: 17 March 2020

The Cryosphere Discussions

First spectral measurements of light attenuation in Greenland Ice Sheet bare ice suggest shallower subsurface radiative heating and ICESat-2 penetration depth in the ablation zone

Matthew G. Cooper[1], Laurence C. Smith[2,3], Asa K. Rennermalm[4], Marco Tedesco[5,6], Rohi Muthyala[4], Sasha Z. Leidman[4], Samiah E. Moustafa[2], Jessica V. Fayne[1]

[1]Department of Geography, University of California, Los Angeles, Los Angeles, 90027, USA
[2]Institute at Brown for Environment and Society, Brown University, Providence, 02912, USA
[3]Department of Earth, Environmental and Planetary Sciences, Brown University, Providence, 02912, USA
[4]Department of Geography, Rutgers University, Piscataway, 08854, USA
[5]NASA Goddard Institute for Space Studies, New York, 10025, USA
[6]Lamont Doherty Earth Observatory, Columbia University, New York, 10964, USA

Correspondence to: Matthew G. Cooper (guycooper@ucla.edu)

Abstract. Light transmission into bare glacial ice affects surface energy balance, bio-photochemical cycling, and light detection and ranging (LiDAR) laser elevation measurements but has not previously been reported for the Greenland Ice Sheet. We present in-ice solar irradiance measured over the spectral range 350–900 nm and 12–77 cm depth collected at a site in the western Greenland ablation zone. The acquired spectral irradiance measurements are used to calculate flux attenuation coefficients using an exponential decay Bouguer law model and are compared to values calculated from two-stream radiative transfer theory. Relative to asymptotic two-stream theory, our empirical attenuation coefficients are up to one order of magnitude larger in the range 350–530 nm, suggesting light absorbing particles embedded in ice enhance visible light absorption at our field site. The empirical coefficients accurately describe light attenuation in the ice interior but underestimate light attenuation near the ice surface. Consequently, Bouguer's law overestimates transmitted flux by up to 50% depending on wavelength. Refraction is unlikely to explain the discrepancy. Instead, vertical variation in the ice microstructure and the concentration of light absorbing particles appears to enhance near-surface attenuation at our field site. The magnitude of this near-surface attenuation implies that optical penetration depth is lower by up to 19 cm (28%) at wavelengths relevant to visible-wavelength lidar altimetry of ice surface elevation (e.g. 532 nm for the Ice, Cloud, and Land Elevation Satellite-2) than is suggested by e-folding depths inferred from two stream theory for optically pure glacier ice. This enhanced near-surface attenuation implies shallower light transmission and therefore lower subsurface light availability for subsurface radiative heating and bio-photochemical cycling. We recommend radiative transfer models applied to bare ice in the Greenland Ice Sheet ablation zone account for vertical variation in light attenuation due to the vertical distribution of light absorbing particles and ice microstructure, and we provide new values of flux attenuation, absorption, and scattering coefficients to support model validation and parameterization.

https://doi.org/10.5194/tc-2020-53
Preprint. Discussion started: 17 March 2020


The Cryosphere Discussions

1 Introduction

Understanding the transmission, absorption, and scattering of light in ice is important for snow and ice energy balance modelling (Brandt and Warren, 1993), lidar remote sensing of snow surface elevation and grain size (Deems et al., 2013; Yang et al., 2017), primary productivity beneath sea ice (Frey et al., 2011; Grenfell, 1979), bio-photochemical cycling in ice and snow (France et al., 2011), and theoretical predictions of "Snowball Earth" paleoclimates (Dadic et al., 2013; Warren et al., 2002). Each of these applications requires knowledge of the vertical distribution of light attenuation in ice, which for a medium (such as glacier ice) that both absorbs and scatters light is specified by the spectral flux attenuation coefficient:

$$k_{\mathrm{att}} = k_{\mathrm{abs}} + k_{\mathrm{scat}} \quad (1)$$

where k_{abs} [m^{-1}] is the spectral flux absorption coefficient, k_{scat} [m^{-1}] is the spectral flux scattering coefficient, and all are functions of wavelength, λ. This study reports on k_{att} of bare glacier ice in the Greenland Ice Sheet ablation zone, a critical parameter needed to calculate subsurface absorption and backscattering of transmitted radiation that to our knowledge has received no direct field study.

Measurements of k_{att} in snowpack and sea ice indicate three main sources of variation with relevance to geophysical applications. First, the magnitude of k_{att} is primarily controlled by ice microstructure via its control on k_{scat}, which for the range of air bubble and ice grain sizes observed in natural snow and ice is nearly independent of wavelength (Perovich, 1996). Spectrally, k_{att} is low in the near-ultraviolet and blue-green spectral region (~250–600 nm) where k_{abs} is extremely low (<10^{-8}), and progressively higher for wavelengths >600 nm, where k_{abs} rapidly increases up to its maximum value (~10^{-2}) at the far end of the solar spectrum (Warren and Brandt, 2008). Vertically, k_{att} is at a maximum at the incident boundary (the snow or ice surface) where a significant portion of upwelling radiation (i.e. transmitted flux reflected upwards) escapes the ice volume before re-reflection downward. Within this near-surface optical boundary layer (Bohren and Barkstrom, 1974), attenuation rates rapidly decrease with depth to an asymptotic value as multiple scattering establishes an isotropic (diffuse) radiation field (Briegleb and Light, 2007; Warren, 1982). For fine-grained dry snow, a few cm depth is typically sufficient to reach the "diffuse" asymptotic regime where k_{att} is constant (Brandt and Warren, 1993). For sea ice the depth required is typically larger and can exceed >20 cm depending on near-surface ice microstructure and the vertical location of the refractive boundary if present (Grenfell, 1991; Grenfell and Maykut, 1977). Attenuation coefficients are also influenced by the horizontal distribution of ice type and surface cover (Frey et al., 2011) but this source of variation is not examined here.

In addition to experimental values obtained from measurements of light transmission in ice or snow, k_{att} is obtained analytically from optical theory (Bohren, 1987; Warren et al., 2006). Light attenuation in pure ice is specified analytically by the complex index of refraction $m(\lambda) = m_{\mathrm{re}} - \mathrm{i}\, m_{\mathrm{im}}$, where m_{re} is the real refractive index (~1.31 in the visible), m_{im} is the imaginary index, λ is wavelength, and $k_{\mathrm{abs,ice}} = 4\pi\lambda^{-1} m_{\mathrm{im}}$ is the absorption coefficient of pure ice (Warren et al., 2006; Warren and Brandt, 2008). Light attenuation in glacier ice differs from pure ice owing to compositional and structural factors

https://doi.org/10.5194/tc-2020-53
Preprint. Discussion started: 17 March 2020


The Cryosphere Discussions
Open Access
EGU

that control scattering and absorption, such as the size, geometry, and vertical distribution of embedded light absorbing particles (LAPs) and light scattering air bubbles and ice grains of size > wavelength (Askebjer et al., 1997; Picard et al., 2016; Price and Bergström, 1997; Warren et al., 2006). Analytical methods typically assume ice and snowpack can be approximated as homogeneous plane-parallel slabs of spherical ice grains and/or air bubbles, for which Mie theory is used to calculate single-scattering properties and two-stream radiative transfer theory is used to calculate multiple scattering and bulk absorption in the ice volume. Such models have been used to calculate subsurface meltwater production caused by penetration of solar radiation in ice both in Greenland (van den Broeke et al., 2008; Kuipers Munneke et al., 2009) and Antarctica (Brandt and Warren, 1993; Hoffman et al., 2014; Liston et al., 1999a, 1999b; Liston and Winther, 2005). However, theoretical values for k_{att} used as input to such models are rarely validated experimentally, and to our knowledge no such experimental values exist for glacier ice.

In addition to ice surface energy balance, understanding light attenuation in ice is important for interpreting interactions between visible-wavelength light sources and ice surfaces, for example laser altimetry measurements of ice surface elevation (Deems et al., 2013; Gardner et al., 2015; Greeley et al., 2017). The reciprocal of k_{att} is the attenuation length, or the average distance travelled by a photon before attenuation by absorption or scattering (Ackermann et al., 2006). In the context of altimetry, the attenuation length is sometimes referred to as the penetration depth, or the average depth to which the electromagnetic signal penetrates before it is backscattered to the atmosphere (Ridley and Partington, 1988; Rignot et al., 2001; Zebker and Weber Hoen, 2000). The laser altimeter onboard Ice, Cloud, and Land Elevation Satellite-1 (ICESat-1) transmitted 1064 nm laser pulses to measure the distance (range) between the satellite and ice sheet surfaces (Schutz et al., 2005). Photons with wavelength 1064 nm penetrate snowpack no more than a few centimetres (Brandt and Warren, 1993; Järvinen and Leppäranta, 2013). This length scale is smaller than typical laser altimetry surface elevation errors due to ice and snow surface roughness and geolocation uncertainty (Deems et al., 2013). In contrast, the laser altimeter onboard ICESat-2 transmits 532 nm laser pulses (Markus et al., 2017). Ice is ~10× more transparent at 532 nm than at 1064 nm (Warren and Brandt, 2008), and photons at 532 nm may penetrate many tens of centimetres into glacier ice. These subsurface scattered photons may introduce a range bias in ICESat-2 surface elevation retrievals over glacier ice, similar to radar penetration into snow (Brunt et al., 2016; Gardner et al., 2015; Greeley et al., 2017). To our knowledge no in situ observations of 532 nm optical penetration depth for bare glacier ice exist, thereby precluding field validation of penetration depth obtained from theoretical radiative transfer models.

The purpose of this investigation is to provide experimental values for k_{att} obtained from measurements of solar flux attenuation in bare ice in the Greenland Ice Sheet ablation zone, and to compare them with theoretical values for k_{att} obtained from the two-stream analytical solution (c.f. Eq. 26 Bohren, 1987; Schuster, 1905). We benchmark our field estimates against the two-stream solution because of its wide use in surface energy balance models applied to snow and ice. In Sect. 2 we describe the field measurements and the optical theory used to interpret the solar flux attenuation. In Sect. 3 we report values

https://doi.org/10.5194/tc-2020-53
Preprint. Discussion started: 17 March 2020


The Cryosphere Discussions

for k_{att} and k_{abs} obtained from our measurements, compare them with values obtained from two-stream theory, and propose a simple empirical model that accounts for enhanced near-surface attenuation. In Sect. 4 we discuss how our k values differ from prior experimental values acquired in sea ice and snowpack and from theoretical values, and the implication of these differences for modelling radiative transfer in bare glacier ice. To demonstrate the broader implications of our study, we suggest how our findings can be used to understand interactions between visible-light laser altimetry (e.g. ICESat-2) and bare glacial ice surfaces, and how they can be used to improve models for subsurface heating of ablating glacier ice.

2 Methods

2.1 Transmittance measurements

Ice transmittance was measured on 20 July 2018 in the Kangerlussuaq sector of the western Greenland Ice Sheet. The study site (67.15 ºN, 50.02 ºW) is located ~1 km from the ice sheet margin at 840 m a.s.l. Subsurface (in-ice) spectral irradiance was measured at 0.35 nm spectral resolution in the wavelength range 300–900 nm with an Ocean Optics® JAZ spectrometer calibrated for absolute irradiance. Light was guided from the ice interior to the spectrometer with a 3 mm diameter Kevlar-sheathed fibre optic cable fitted inside a 2 m long insulated white PVC tube (Figure 1). The fibre was affixed at one end to a Spectralon remote cosine receptor (RCR) diffuser via a 90º collimating lens adapter. The RCR barrel was wrapped in white PTFE tape and set 2 mm out from the PVC tube exterior to act as a contact horizon between its diffusing element and the ice. The system was operated from a battery-powered computer running the Ocean Optics Ocean View software. The computer and spectrometer were placed on a tripod platform oriented 180º away from the sun and 2.5 m horizontal distance from the measurement location.

To access the interior of the ice, holes were drilled horizontally into a 2-m high sidewall of a natural ice feature with a battery powered hand drill fitted with a 3 cm diameter Kovacs auger bit. Each hole was drilled 2 m deep into the ice. Starting at the lowest hole near the bottom of the sidewall, the auger was advanced into the sidewall approximately 20 cm, levelled horizontally with a digital spirit level, and the sequence repeated to 2 m horizontal depth. The PVC tube-fibre optic assembly was then inserted into the hole, RCR facing upward, and a 2 m long ruler was shimmed under the bottom of the PVC tube to ensure the RCR barrel preserved contact with the overlying ice thus minimizing stray light contamination into the RCR field of view. Ice shavings were packed around the drill hole to prevent light reflection into the hole. Spectral irradiance was recorded at 1 Hz frequency using a 20-scan average and 44 Hz integration time for 30 seconds yielding 30 irradiance profiles, after which the tube was removed, the next hole was drilled, and the sequence was repeated working from the bottom toward the ice surface.

Background upwelling and downwelling spectral irradiance were measured continuously at 2 m height above the ice surface approximately 3 m away from the in-ice measurements using a dual-channel Ocean Optics JAZ spectrometer calibrated for

https://doi.org/10.5194/tc-2020-53
Preprint. Discussion started: 17 March 2020


The Cryosphere Discussions
Open Access
EGU

130 absolute irradiance. These data were recorded at 1 min frequency using a 20-scan average and 92 Hz integration time. Light was guided to the spectrometer via two 3 m fibre optic cables attached to two RCRs mounted in upward-looking and downward-looking orientation on a 2 m long horizontally levelled boom attached to a vertical mast drilled into the ice. The measurements were completed between 13:45 and 14:35 local time (UTC -3), at solar zenith angles of ~48–51°. Solar noon at this time and location is ~13:26.

135 **2.2 Experimental determination of asymptotic flux attenuation coefficients**

Spectral asymptotic flux attenuation coefficients are estimated by fitting a Bouguer-law exponential decay model as per Grenfell and Maykut (1977) to the in-ice irradiance depth profiles:

$$\mathrm{I}(\mathrm{z},\lambda) = \mathrm{I}(\mathrm{z_o},\lambda)\mathrm{e}^{-k_{\mathrm{att}}(\lambda)(\mathrm{z}-\mathrm{z_o})} \quad (2)$$

where $k_{\mathrm{att}}(\lambda)$ is the asymptotic flux attenuation coefficient for wavelength λ, $\mathrm{I}(\mathrm{z})$ is in-ice spectral irradiance at depth z, $\mathrm{I}(\mathrm{z_o})$ is background downwelling spectral irradiance, $\mathrm{z_o}$ is the ice surface, and $T(\mathrm{z},\lambda) = \mathrm{I}(\mathrm{z},\lambda)/\mathrm{I}(\mathrm{z_o},\lambda)$ is spectral transmittance.

140 The raw 0.35 nm spectra were interpolated to 1 nm using bilinear interpolation and smoothed with a centred moving mean filter with window size 3 nm. Estimates of $k_{\mathrm{att}}(\lambda)$ for each 1 nm band were estimated as the slope of the ordinary least-squares linear solution to $\ln T(\mathrm{z},\lambda)$ vs. $(\mathrm{z}-\mathrm{z_o})$.

The optical depth $\tau(\mathrm{z},\lambda)$ is a dimensionless path length that scales the physical thickness of a layer by its attenuation rate:

$$\tau(\mathrm{z},\lambda) = \mathrm{k_{att}}(\lambda)\cdot\mathrm{z} = -\ln \mathrm{T}(\mathrm{z},\lambda) \quad (3)$$

145 The attenuation length $l(\lambda)$ is the inverse of $k_{\mathrm{att}}(\lambda)$, and is referred to elsewhere as the photon mean free path (Ackermann et al., 2006). It is equivalent to the path length in ice required to attenuate irradiance to 37% ($1/e$) of its incident intensity, i.e. the path length at which $T = 1/e$ and $\tau = 1$:

$$l(\lambda) = \frac{1}{k_{\mathrm{att}}(\lambda)} \quad (4)$$

Note that attenuation is expressed in terms of $l(\lambda)$ in Sect. 3.4 and 4.3 to describe its physical in-situ length-scale. Solid ice-equivalent values of $k_{\mathrm{att}}(\lambda)$, $k_{\mathrm{abs}}(\lambda)$, and $k_{\mathrm{scat}}(\lambda)$ are provided in Appendix 1.

150 **2.3 Theoretical determination of asymptotic flux attenuation coefficients**

Theoretical values of $k_{\mathrm{att}}(\lambda)$ are calculated using the solution given by the two-stream radiative transfer approximation (Schuster, 1905):

$$k_{\mathrm{att}}(\lambda) = \frac{3}{4}\frac{\rho_{\mathrm{i}}}{\rho_{\mathrm{ice}}}\frac{Q_{\mathrm{ext}}(\lambda)}{r_{\mathrm{eff}}}\sqrt{(1-\omega(\lambda))(1-g\omega(\lambda))} \quad (5)$$

https://doi.org/10.5194/tc-2020-53
Preprint. Discussion started: 17 March 2020

where ρ_i is ice sample density (kg m^{-3}), ρ_{ice} is pure ice density (917 kg m^{-3}), $Q_{ext}(\lambda)$ is the extinction efficiency, r_{eff} is the effective scattering particle radius (m), $g(\lambda)$ is the average cosine of the scattering angle, and $\omega(\lambda)$ is the single-scattering albedo. Eq. (5) describes light attenuation by multiple scattering and absorption in a homogeneous plane-parallel slab of absorbing spheres. Its derivation is available in Bohren (1987).

To estimate r_{eff}, Eq. (5) is iteratively solved for the value of r_{eff} that minimizes the difference between measured and calculated k_{att} at $\lambda = 600$ nm. This method assumes all absorption at 600 nm is due to ice (Warren et al., 2006). If absorption was influenced by LAPs r_{eff} would be over-estimated. Values for $Q_{ext}(\lambda)$, $g(\lambda)$, and $\omega(\lambda)$ are obtained from Mie scattering algorithms provided as MATLAB code by Mätzler (2002), $m(\lambda)$ is from Warren and Brandt (2008), and ρ_i is obtained from an ice core extracted at the measurement location with depth-weighted measured ice density 835 kg m^{-3}. The optimal r_{eff} value is 2.8 mm and this value is used in all subsequent calculations.

2.4 Flux absorption coefficients

Warren et al. (2006) developed a method to estimate $k_{abs,ice}(\lambda)$ from measurements of flux attenuation in snow in Antarctica. The method relies on three assumptions: 1) the value of $k_{abs,ice}$ at 600 nm is known accurately, 2) the value of k_{abs} at 600 nm is not affected by LAPs in the measured snow or ice, and 3) $\omega(\lambda)$ varies so little as to be effectively independent of wavelength in the spectral range considered (here the near-UV and visible). Warren et al. (2006) verified the validity of these assumptions for the spectral range 350–600 nm and obtained the following relation (Eq. 15 of that paper) between flux attenuation and flux absorption:

$$\left[\frac{k_{att}(\lambda)}{k_{att}(\lambda_o)}\right]^2 \approx \left[\frac{k_{abs}(\lambda)}{k_{abs}(\lambda_o)}\right] \quad (6)$$

where $\lambda_o = 600$ nm is the reference wavelength. Eq. (6) was used by Warren et al. (2006) to estimate k_{abs} for pure ice (i.e. $k_{abs,ice}$) from 350–600 nm.

Eq. (6) requires that absorption at the reference wavelength (600 nm) is not affected by LAPs but the relation can be used to estimate k_{abs} at any other wavelength, including those where absorption is affected by LAPs. At those wavelengths, Eq. (6) will predict values for k_{abs} higher than those for pure ice if LAPs are present in the measured snow or ice volume, due to the influence of LAPs on k_{att}. Consequently, although not developed for this purpose, Eq. (6) provides a means to infer the influence of LAPs on measured flux attenuation by comparison with values of $k_{abs,ice}$ provided by Warren et al. (2006), which are compiled in Brandt and Warren (2008). A similar approach was used to infer LAP absorption in snowpack (Tuzet et al., 2019). Here, we exploit this to interpret differences between our theoretical and experimental values of k_{att} on the basis of differences between $k_{abs,ice}$ (Warren et al., 2006) and the k_{abs} values that we obtain for glacier ice from Eq. (6).

https://doi.org/10.5194/tc-2020-53
Preprint. Discussion started: 17 March 2020


The Cryosphere Discussions

2.5 Near surface effects

The $k_{att}(\lambda)$ values calculated using Eq. (2) are applicable at distances far enough from the incident boundary (here the ice surface) that the radiation field is diffuse and $k_{att}(\lambda)$ is constant with depth. Near the ice surface the radiation field is converted via multiple scattering from direct to diffuse flux, and attenuation is enhanced by transmission of upward reflected light out of the ice volume before re-reflection downward (Briegleb and Light, 2007). Attenuation may also be enhanced by specular reflection at the ice surface, depending on its roughness (Dadic et al., 2013; Mullen and Warren, 1988). To parameterize these near-surface effects, we introduce a modified form of Eq. (2):

$$I(z,\lambda) = (1-\chi)\, I(z_o,\lambda) e^{-k_{att}(\lambda)(z-z_o)} \quad (7)$$

where χ is the fraction of incident spectral irradiance attenuated in the near-surface boundary layer (inclusive of the surface) and all other terms are as previously defined. The χ parameter is analogous to the i_o parameter introduced by Grenfell and Maykut (1977) to partition the bulk (spectrally-integrated) net absorbed solar flux between the upper 10 cm of sea ice, which they termed the "Surface Scattering Layer" (SSL), and the ice interior, in which radiation is exponentially attenuated at a constant rate. The i_o parameter has been widely adopted in energy balance models of glaciers and sea ice where radiation penetration is important (Bintanja and Van Den Broeke, 1995; Hoffman et al., 2014; Holland et al., 2012). For example, the sea ice component of the Community Earth System Model (CESM) uses $i_o = 30\%$ (Briegleb and Light, 2007). The important distinction is that i_o is a spectrally integrated value applicable to energy balance modelling whereas χ is applicable for comparison with measurements of downward spectral irradiance within ice.

3 Results

3.1 Spectral transmittance measurements

Four spectra of in-ice irradiance were collected at 12 cm, 36 cm, 58 cm, and 77 cm depth below the ice surface (Figure 2a). These spectra are normalized by the coincident-in-time surface spectra to calculate spectral transmittance, T (Figure 2c). At all depths, T is maximum at 430 nm and maintains relatively stable and high values up to about 500 nm in the visible, beyond which T decreases into the red end of the visible spectrum where absorption by ice is higher. Maximum T values vary from 78% at 12 cm to 41% at 77 cm. For $\lambda > 500$ nm T rapidly decreases both with wavelength and with depth. Beyond about 800 nm nearly all incident light is attenuated below 36 cm, with T<2% at 36 cm and <0.6% at 58 and 77 cm depth. In contrast, T at 12 cm decreases from 18% at 800 nm to 5% at 900 nm, suggesting substantial subsurface flux absorption in the 12–36 cm depth region (Figure 2c).

3.2 Field estimates of flux attenuation coefficients and albedo

Example log-linear fits to Eq. (2) at $\lambda = 350, 450, 550, 650,$ and 700 nm give k_{att} values ranging from 1.03 m^{-1} to 5.51 m^{-1} (Figure 3a). These values correspond to attenuation lengths of 0.97 m to 0.18 m, respectively. Measured values of in-ice

https://doi.org/10.5194/tc-2020-53
Preprint. Discussion started: 17 March 2020


The Cryosphere Discussions

irradiance at 58 cm and 77 cm depth were too low to calculate k_{att} beyond 700 nm (Figure 2 and Figure 3c). Although T is maximum at 430 nm, the minimum k_{att} value (0.96 m^{-1}) occurs at 396 nm. The coefficient of determination (r^2) ranged from 0.96–1.0 ($p<0.01$), with a median value of 0.98, suggesting the data are described appropriately by the Bouguer-law exponential decay model.

Albedo spectra correspond closely to patterns in transmittance and k_{att} spectra (Figure 3c). The near-UV and blue wavelengths that efficiently transmit into ice mostly re-emerge as reflected light, owing to the extremely low values of ice absorption coefficient in the wavelength range 350–500 nm where albedo is maximum (Warren et al., 2006). The maximum measured albedo value (0.83) occurs at 447 nm, suggesting a slight red shift relative to the location of the minimum k_{att} value (0.96 m^{-1}) at 396 nm, however albedo varies little in the region of minimum k_{att} and is 0.82 at 396 nm. Beyond about 500 nm, albedo decreases rapidly, and most transmitted light is absorbed, as indicated by the larger k_{att} values and the extremely low transmittance at depths below 36 cm.

3.3 Theoretical flux attenuation coefficients

Theoretical k_{att} values predicted by the two-stream solution are nearly one order of magnitude lower than field estimates of k_{att} for $\lambda < 500$ nm (blue circles vs orange line, Figure 4a). This discrepancy can be inferred to relate to the presence of LAPs embedded in the ice matrix that increase the effective absorption of the ice volume. For example, differences between the field-estimate of k_{abs} and $k_{abs,ice}$ (Figure 4b) mirror those between the field-estimate and theoretical estimate of k_{att} (Figure 4a). Namely, k_{abs} is nearly one order of magnitude larger than $k_{abs,ice}$ in the range 350–500 nm, where even very small concentrations of LAPs in the measured ice volume would dominate absorption (Warren et al., 2006). In contrast, the two-stream solution and theory converge at $\lambda > 530$ nm where absorption is dominated by grain-size effects.

To gain further insight into the mechanisms that drive differences between field estimates and two-stream theory, we compare our k_{att} values for glacier ice in Greenland to published values of k_{att} for clean, fine-grained snow in Antarctica ($k_{att,snow}$) (Warren et al., 2006) (Figure 5). The values for $k_{att,snow}$ reported by Warren et al (2006) were obtained by applying Eq. 1 to measurements of flux transmission in a ~45 cm thick snow layer at ~90–135 cm depth near Dome C (75°S, 123°E, 3230 m), adjusted to remove the absorptive influence of ~0.3 ppb soot (the radiative forcing of 0.3 ppb soot is equivalent to a 4 um increase in r_{eff}). These values are therefore representative of flux attenuation in optically pure snow. We also calculate $k_{att,snow}$ using Eq. (5) with values for r_{eff} (135 um) and ρ_i (463 kg m^{-3}) as reported by Warren et al (2006).

Because scattering is a function of r_{eff} but independent of λ, the curves for $k_{att,snow}$ and $k_{att,ice}$ (blue circles vs purple squares, Figure 4a) have a constant offset proportional to the ratio $r_{eff,snow}/r_{eff,ice}$ (c.f. Eq. 16 of Warren et al., 2006). This holds true when considering structural differences between snow and ice that control scattering (i.e. snow grains vs air bubbles) since

https://doi.org/10.5194/tc-2020-53
Preprint. Discussion started: 17 March 2020

$r_{\text{eff}} \gg \lambda$ in either case. In contrast, field estimates for glacier ice clearly diverge from theoretical estimates with a wavelength-dependent offset in the spectral range 350–530 nm where LAPs dominate absorption (blue circles vs. orange line, Figure 4a). Finally, it is evident that scattering by fine-grained snow greatly enhances flux attenuation. This comparison provides a useful contrast between the flux attenuation properties of snow vs glacier ice that is discussed in Sect. 4.

3.4 Transmitted irradiance and near-surface attenuation

Near the ice surface irradiance is not attenuated exponentially and Bouguer's law does not hold, as confirmed by the y-intercepts of the straight lines in Fig. 3b at values <100%. This suggests k_{att} values are higher in the 0–12 cm near-surface region where irradiance measurements were not obtained. Consequently, transmitted irradiance is overestimated by 5–50% if Bouguer's law is applied to the incident surface irradiance using k_{att} values from the 12–77 cm region, with median over-estimation 16% (Figure 5a). The value of χ (Eq. (7) that minimizes the root-mean-squared-difference between measured and predicted transmitted irradiance, weighted equally at all depths and all λ, is 15%. Transmitted irradiance spectra predicted using Eq. (7) with $\chi = 15\%$ are shown in Figure 5c.

Expressed in terms of attenuation rate, effective k_{att} values for the 0–12 cm region estimated from a finite-difference solution to Eq. (2) are ~1.5× higher than those in the 12–77 cm region for $\lambda > 570$ nm, and are up to 3.7× higher between 400–570 nm (Figure 6). This suggests attenuation enhancement by LAPs is higher in the 0–12 cm region than in the 12–77 cm region, consistent with the expectation that impurity concentration is higher near the ice surface. Stated in terms of attenuation length, l varies from 117 cm at 356 nm to 14 cm at 700 nm. These values are calculated by combining the effective k_{att} values for the 0–12 cm region with the k_{att} values for the 12–77 cm region and therefore correspond to effective penetration depths. Effective penetration depths are smaller than attenuation lengths inferred from k_{att} values for the 12–77 cm region (i.e. from Eq. 4), owing to the higher attenuation in the 0–12 cm region. The effective penetration depth at 532 nm is 49 cm, or 15 cm lower than the 64 cm attenuation length implied by our empirical k_{att} values in the 12–77 cm region, and 19 cm lower than the 68 cm attenuation length implied by theoretical k_{att} values for optically pure glacier ice.

The enhanced near-surface attenuation found here is consistent with observations of enhanced attenuation in the granular and porous surface layer on sea ice (Grenfell and Maykut, 1977). The field measurements were collected following several days of light but persistent rainfall and cloud cover, conditions that inhibit development of granular near-surface ice (e.g. 'weathering crust') (Müller and Keeler, 1969). Qualitatively, the ice surface was semi-granular to a depth of ~4 cm, below which the ice transitioned to solid bubbly ice (Figure 7). For example, the upper four centimetres of ice core could not be recovered owing to its granular structure. The recovered core was split into three segments corresponding to depths of 4–45 cm, 45–74 cm, and 74–122 cm below the ice surface. The density of these segments was 801 kg m^{-3}, 884 kg m^{-3}, and 888 kg

https://doi.org/10.5194/tc-2020-53
Preprint. Discussion started: 17 March 2020


The Cryosphere Discussions

m^{-3}, respectively. An ice screw was used to recover an ice sample from the upper 8 cm. The density of this ice was 699 kg m^{-3}, confirming the presence of low-density granular near-surface ice.

For smooth ice surfaces, attenuation may be enhanced by refraction at the ice-air interface (Mullen and Warren, 1988). If present, a refractive boundary would enhance near-surface attenuation via external specular reflection, and possibly via enhanced near-surface absorption of the internally reflected downward flux. Following Briegleb and Light (2007), we calculate the external diffuse specular reflectivity for a flat ice surface to be 0.063, meaning specular reflection could enhance attenuation by up to 6.3%. This value is smaller than the 10–25% surface attenuation implied by the y-intercepts in Figure 3c, suggesting specular reflection alone cannot explain the discrepancy. Instead, we suggest that enhanced scattering by the granular near-surface ice microstructure, together with absorptive impurities, enhanced near-surface light attenuation at our field site.

3.5 Uncertainty analysis

We repeated the entire analysis reported in Sect. 3 using $\rho_i = 801\ \mathrm{kg\ m^{-3}}$ and $\rho_i = 884\ \mathrm{kg\ m^{-3}}$, values that bracket the range of ice density measured in the ice interior. The optimal r_{eff} values were 2.5 mm and 3.2 mm, respectively. However, the single-scattering properties varied so little (max difference 0.2% for $\omega > 800$ nm) that all reported results were identical. The ice-equivalent k_{att} values given in Appendix 1 are referenced to the depth-weighted ice density measured in the 4–74 cm region (835 kg m^{-3}). The reader is advised that ice density varied from 801–884 kg m^{-3} between 4–122 cm depth; however, this analysis reports on measurements collected between 12–77 cm depth, for which ice density varied from 801–842 kg m^{-3}.

Two separate observers made ten independent measurements of the vertical distance between the in-ice irradiance collections. The mean error ($\pm$ one standard deviation) was 0.9 ± 1.2 cm. During the period 19–22 July one of these observers measured the height of an ablation stake using the same ruler that was used to measure the vertical distance between the in-ice irradiance collections. Two measurements were taken each time, for 41 total replicates. The mean error ($\pm$ one standard deviation) was 0.2 ± 1.2 cm. This suggests 1.2 cm is a reasonable approximation for vertical measurement uncertainty, and is represented as horizontal uncertainty bars on the in-ice transmittance values in Figure 3b and as shaded uncertainty bounds on the near-surface attenuation rates in Figure 6.

4 Discussion

4.1 Comparison with attenuation spectra for sea ice and snowpack

We report first spectral measurements of near-UV and visible light transmission in bare ablating glacier ice. These measurements are used to estimate asymptotic flux attenuation coefficients k_{att} for the spectral range 350–700 nm. Prior studies quantified k_{att} for sea ice (c.f. Frey et al., 2011; Grenfell and Maykut, 1977; Light et al., 2008; Pegau and Zaneveld,

https://doi.org/10.5194/tc-2020-53
Preprint. Discussion started: 17 March 2020

2000), snowpack (Fisher et al., 2005; Gerland et al., 2000; Järvinen and Leppäranta, 2013; King and Simpson, 2001; Meirold-Mautner and Lehning, 2004; Picard et al., 2016; Tuzet et al., 2019; Warren et al., 2006), and for compressed glacial ice at 800–2350 m depth in the Antarctic Ice Sheet for which optical scattering is not representative of near-surface ablating glacier ice (Ackermann et al., 2006; Askebjer et al., 1995, 1997).

Light attenuation in glacier ice differs from sea ice and snowpack in several important ways. Figure 8 compares the k_{att} spectra for glacier ice measured here to seven previously published k_{att} spectra for snowpack and sea ice. Light attenuation in sea ice is controlled by its unique vertical composition, including brine inclusions, air pockets, solid salts, sea ice algae, dissolved organic matter, and radiative interactions between the ice and underlying ocean (Perovich, 1996). Relative to prior measurements in sea ice (Grenfell et al., 2006; Grenfell and Maykut, 1977), our results suggest light attenuation by glacial ice is lower at blue-green wavelengths and higher at orange-red wavelengths, likely reflecting differences in the absorption spectra of light absorbing material found in sea ice relative to that found in glacier ice (Figure 8). Relative to prior measurements made in snow near Summit, Greenland (Meirold-Mautner and Lehning, 2004), our results suggest attenuation by glacial ice has a similar spectral shape but lower attenuation at all wavelengths, likely due to enhanced scattering from the fine-grained structure of polar snow. Snow near Dome-C in Antarctica has lower attenuation at blue-green wavelengths than snow near Summit, Greenland, but is nearly identical at longer wavelengths, suggesting visible-light attenuation at Summit is enhanced by higher LAP concentration. Attenuation within the surface scattering layer (SSL) of sea ice is higher still, and attenuation at 5 cm depth in snow near Summit is highest of all, likely due to direct scattering of light out of the near-surface optical boundary layer. The comparison demonstrates the tremendous variation in k_{att} values caused by differences in ice structure and composition, and the importance of site-specific studies such as ours for characterization of ice optical properties.

4.2 Relevance to surface energy balance modelling and subsurface meltwater production

Our field estimates of k_{att} are up to one order of magnitude larger in the spectral range 350–530 nm than those obtained from two-stream theory for optically clean ice. This is important because visible light transmission provides an energy source for subsurface heating and internal melting of glacier ice in the ablation zones of glaciers and ice sheets (Cooper et al., 2018; Hoffman et al., 2014; Liston and Winther, 2005; Schuster, 2001). Prior estimates of subsurface meltwater production in bare ice used two-stream theory forced by values of $m(\lambda)$ for pure ice to calculate k_{att} and the absorbed solar flux as a function of depth below the ice surface in both Greenland and Antarctica (van den Broeke et al., 2008; Hoffman et al., 2014; Kuipers Munneke et al., 2009; Liston and Winther, 2005). Comparison with the spectral absorption coefficient of pure ice (Figure 4c) suggests the discrepancy we find is likely due to LAPs present in the measured ice volume, which appear to disproportionately enhance energy absorption near the ice surface.

Examples of LAPs found in near-surface glacier ice include dust, black carbon, and microorganisms such as cyanobacteria and algae, each of which absorb light at wavelengths < ~600 nm (Bøggild et al., 2010; Ryan et al., 2018; Stibal et al., 2017;

https://doi.org/10.5194/tc-2020-53
Preprint. Discussion started: 17 March 2020

Takeuchi, 2002; Warren et al., 2006; Yallop et al., 2012). To our knowledge, the influence of LAPs on subsurface meltwater production has not been quantified and is beyond our scope here, but our results point to the potential for subsurface energy absorption enhancement by LAPs in ablating glacier ice. This is consistent with inferences made for surface melt rates caused by distributed LAPs on bare ice surfaces in Greenland (Bøggild et al., 1996; Goelles et al., 2015; Goelles and Bøggild, 2017), and for subsurface energy absorption in snowpack (Tuzet et al., 2019). Moreover, if present in higher concentration near the ice surface, LAPs would reduce light availability for subsurface heating at depth. This is supported by the enhanced attenuation rates found at wavelengths between 400–570 nm for the 0–12 cm region relative to those for the 12–77 cm interior ice region (Figure 6b).

4.3 Relevance of enhanced near-surface attenuation to ICESat-2

Our results suggest penetration depth of visible wavelength light into solid glacier ice is lower by up to 19 cm at wavelengths relevant to visible-wavelength lidar altimetry of ice surface elevation (e.g. 532 nm for the Ice, Cloud, and Land Elevation Satellite-2). Our asymptotic k_{att} values suggest e-folding penetration depth (the physical depth in units of ice thickness equivalent to one optical depth; equivalently, the physical depth required to attenuate incident irradiance to $1/e$ or ~37%) at 532 nm is 64 cm, in relatively close agreement with two-stream theory that predicts 68 cm. However, this path length is only relevant at depths within the ice volume where the light field is diffuse and attenuation rates are asymptotic (Briegleb and Light, 2007). Near the ice surface attenuation rates are enhanced and rapidly decrease to their asymptotic value. The net effect at our field site is to reduce 532 nm penetration depth to ~49 cm. This enhanced near-surface attenuation is expected, but its magnitude has not previously been measured in near-surface glacier ice. The optimal value $\chi = 15\%$, which parameterizes the magnitude of enhanced near-surface attenuation relative to the interior asymptotic attenuation rate, is one-half the canonical 30% value used in two-layer sea ice models (Briegleb and Light, 2007; Grenfell and Maykut, 1977). This lower value is consistent with our field observations of an anomalously thin (~4 cm) near-surface weathered ice layer (Figure 7), likely due to several days of persistent rain prior to our field measurements. This suggests penetration depths could be reduced further over heavily weathered ice or impurity-laden ice (for which backscatter magnitude may also be reduced), conditions that are common in the Greenland Ice Sheet ablation zone (Cooper and Smith, 2019; Goelles and Bøggild, 2017; Ryan et al., 2018; Tedstone et al., 2017).

The following caveats are important for interpreting the relevance of this experiment to ICESat-2. This experiment quantified the in-ice attenuation of diffuse solar flux. The ICESat-2 instrument transmits and receives discrete laser pulses over finite timesteps at 0° incidence and records the distribution of single-photon travel times returned through the intervening atmosphere (Markus et al., 2017). The penetration depth values given here are therefore not estimates of ICESat-2 laser penetration depth in glacier ice but provide validation data for radiative transfer models specific to the ICESat-2 measurement problem.

https://doi.org/10.5194/tc-2020-53
Preprint. Discussion started: 17 March 2020

4.4 Suggestions for further work

Our results suggest that existing methods for sea ice radiative transfer modelling are readily applicable to ablating glacier ice (Holland et al., 2012; Light et al., 2004). Observations of non-exponential attenuation in sea ice due to enhanced near-surface scattering and vertical variations in ice microstructure motivated adoption of two-layer and then multi-layer models with vertically-varying inherent optical properties, providing a ready template for the enhanced near-surface attenuation we describe here (Briegleb and Light, 2007; Grenfell, 1991; Grenfell and Maykut, 1977; Light et al., 2003). The simple empirical model we demonstrate (Figure 5) suggests the need for a two-layer approach to modelling light attenuation in glacier ice. Vertical variation in ice microstructure and/or scattering geometry can be approximated by treating g and ω as free parameters (Meirold-Mautner and Lehning, 2004), or by using a similarity approach that infers optimal scattering and absorption coefficient values from co-located observations of albedo and transmittance (Light et al., 2004). The values we report provide a possible first step toward using this approach to diagnose structural controls on albedo and radiative transfer in ablating glacier ice. Finally, the k_{abs} values we report provide new insight into the magnitude of this fundamental but uncertain optical property, and provide support for the lower bound pure ice estimate from Warren *et al* (2006) (Figure 9).

5 Conclusion

We report first in-situ spectral measurements of near-UV and visible light attenuation coefficients k_{att} for near-surface bare glacial ice, collected in the Greenland Ice Sheet ablation zone during July 2018. In general, our empirical k_{att} values are nearly one order of magnitude larger in the range 350–530 nm than predicted by asymptotic two-stream radiative transfer theory using canonical values for the complex index of refraction of pure ice (Warren and Brandt, 2008). This suggests light absorbing particles enhance visible light absorption and reduce optical penetration depth at our field site. The simple Bouguer exponential decay model accurately describes light attenuation in the ice interior but underestimates light attenuation near the ice surface. Consequently, light transmission is overestimated by 5–50% depending on wavelength. This enhanced near-surface attenuation is consistent with observations of enhanced scattering from the semi-granular near-surface ice layer on sea ice and appears to be further enhanced at our field site by light absorbing particles concentrated near the ice surface. The magnitude of this near-surface attenuation suggests that visible-light penetration depth at wavelengths relevant to ice surface laser altimetry (e.g. 532 nm for Ice, Cloud, and Land Elevation Satellite-2) is lower by 19 cm than would be inferred from two stream theory for optically pure glacier ice. This enhanced near-surface attenuation implies shallower light transmission and therefore lower light availability for bio-photochemical cycling and subsurface energy absorption in glacier ice. Further work should quantify the sensitivity of light attenuation to vertical variations in ice microstructure and absorptive impurity concentrations representative of near-surface ice in the Greenland Ice Sheet ablation zone, and we provide new values of flux attenuation, absorption, and scattering coefficients to support model parameterization and validation.

https://doi.org/10.5194/tc-2020-53
Preprint. Discussion started: 17 March 2020

Data availability

The data is hosted by the Pangaea open access data repository and is provided as a supplement to this manuscript in Appendix 1.

Author contribution

M.G. Cooper and L.C. Smith designed the experiment. M.G. Cooper, A.K. Rennermalm, M. Tedesco, R. Muthyala, S.Z. Liedman, and S.E. Moustafa collected the field data. M.G. Cooper performed the data analysis and wrote the manuscript. L.C. Smith, A.K. Rennermalm, M. Tedesco, S.Z. Liedman, and J.V. Fayne edited the manuscript. The authors declare they have no conflict of interest.

Acknowledgements

This project was funded by the NASA Cryosphere Program grant 80NSSC19K0942, managed by Dr. Colene Haffke and Dr. Thomas P. Wagner and a graduate fellowship from the NASA Earth and Space Sciences Fellowship Program managed by Dr. Lin Chambers. We thank Polar Field Services for their field support.

References

Ackermann, M., Ahrens, J., Bai, X., Bartelt, M., Barwick, S. W., Bay, R. C., Becka, T., Becker, J. K., Becker, K.-H., Berghaus, P., Bernardini, E., Bertrand, D., Boersma, D. J., Böser, S., Botner, O., Bouchta, A., Bouhali, O., Burgess, C., Burgess, T., Castermans, T., Chirkin, D., Collin, B., Conrad, J., Cooley, J., Cowen, D. F., Davour, A., Clercq, C. D., Heros, C. P. de los, Desiati, P., DeYoung, T., Ekström, P., Feser, T., Gaisser, T. K., Ganugapati, R., Geenen, H., Gerhardt, L., Goldschmidt, A., Groß, A., Hallgren, A., Halzen, F., Hanson, K., Hardtke, D. H., Harenberg, T., Hauschildt, T., Helbing, K., Hellwig, M., Herquet, P., Hill, G. C., Hodges, J., Hubert, D., Hughey, B., Hulth, P. O., Hultqvist, K., Hundertmark, S., Jacobsen, J., Kampert, K. H., Karle, A., Kestel, M., Kohnen, G., Köpke, L., Kowalski, M., Kuehn, K., Lang, R., Leich, H., Leuthold, M., Liubarsky, I., Lundberg, J., Madsen, J., Marciniewski, P., Matis, H. S., McParland, C. P., Messarius, T., Minaeva, Y., Miočinović, P., Morse, R., Münich, K., Nahnhauer, R., Nam, J. W., Neunhöffer, T., Niessen, P., Nygren, D. R., Olbrechts, P., Pohl, A. C., Porrata, R., Price, P. B., Przybylski, G. T., Rawlins, K., Resconi, E., Rhode, W., Ribordy, M., Richter, S., Martino, J. R., Sander, H.-G., Schlenstedt, S., Schneider, D., Schwarz, R., Silvestri, A., Solarz, M., Spiczak, G. M., et al.: Optical properties of deep glacial ice at the South Pole, Journal of Geophysical Research: Atmospheres, 111(D13), doi:10.1029/2005JD006687, 2006.

Askebjer, P., Barwick, S. W., Bergström, L., Bouchta, A., Carius, S., Coulthard, A., Engel, K., Erlandsson, B., Goobar, A., Gray, L., Hallgren, A., Halzen, F., Hulth, P. O., Jacobsen, J., Johansson, S., Kandhadai, V., Liubarsky, I., Lowder, D., Miller, T., Mock, P. C., Morse, R., Porrata, R., Price, P. B., Richards, A., Rubinstein, H., Schneider, E., Sun, Q., Tilav, S., Walck, C. and Yodh, G.: Optical Properties of the South Pole Ice at Depths Between 0.8 and 1 Kilometer, Science, 267(5201), 1147–1150, doi:10.1126/science.267.5201.1147, 1995.

https://doi.org/10.5194/tc-2020-53
Preprint. Discussion started: 17 March 2020

Askebjer, P., Barwick, S. W., Bergström, L., Bouchta, A., Carius, S., Dalberg, E., Erlandsson, B., Goobar, A., Gray, L., Hallgren, A., Halzen, F., Heukenkamp, H., Hulth, P. O., Hundertmark, S., Jacobsen, J., Kandhadai, V., Karle, A., Liubarsky, I., Lowder, D., Miller, T., Mock, P., Morse, R., Porrata, R., Price, P. B., Richards, A., Rubinstein, H., Schneider, E., Spiering, C., Streicher, O., Sun, Q., Thon, T., Tilav, S., Wischnewski, R., Walck, C. and Yodh, G.: UV and optical light transmission properties in deep ice at the South Pole, Geophysical Research Letters, 24(11), 1355–1358, doi:10.1029/97GL01246, 1997.

Bintanja, R. and Van Den Broeke, M. R.: The Surface Energy Balance of Antarctic Snow and Blue Ice, J. Appl. Meteor., 34(4), 902–926, doi:10.1175/1520-0450(1995)034<0902:TSEBOA>2.0.CO;2, 1995.

Bøggild, C. E., Oerter, H. and Tukiainen, T.: Increased ablation of Wisconsin ice in eastern north Greenland: observations and modelling, Annals of Glaciology, 23, 144–148, doi:10.3189/S0260305500013367, 1996.

Bøggild, C. E., Brandt, R. E., Brown, K. J. and Warren, S. G.: The ablation zone in northeast Greenland: ice types, albedos and impurities, Journal of Glaciology, 56(195), 101–113, doi:10.3189/002214310791190776, 2010.

Bohren, C. F.: Multiple scattering of light and some of its observable consequences, American Journal of Physics, 55(6), 524–533, doi:10.1119/1.15109, 1987.

Bohren, C. F. and Barkstrom, B. R.: Theory of the optical properties of snow, J. Geophys. Res., 79(30), 4527–4535, doi:10.1029/JC079i030p04527, 1974.

Brandt, R. E. and Warren, S. G.: Solar-heating rates and temperature profiles in Antarctic snow and ice, Journal of Glaciology, 39(131), 99–110, doi:10.3189/S0022143000015756, 1993.

Briegleb, P. and Light, B.: A Delta-Eddington Mutiple Scattering Parameterization for Solar Radiation in the Sea Ice Component of the Community Climate System Model, , doi:10.5065/D6B27S71, 2007.

van den Broeke, M. R., Smeets, P., Ettema, J., van der Veen, C., van de Wal, R. and Oerlemans, J.: Partitioning of melt energy and meltwater fluxes in the ablation zone of the west Greenland ice sheet, The Cryosphere, 2(2), 179–189, doi:10.5194/tc-2-179-2008, 2008.

Brunt, K. M., Neumann, T. A., Amundson, J. M., Kavanaugh, J. L., Moussavi, M. S., Walsh, K. M., Cook, W. B. and Markus, T.: MABEL photon-counting laser altimetry data in Alaska for ICESat-2 simulations and development, The Cryosphere, 10(4), 1707–1719, doi:10.5194/tc-10-1707-2016, 2016.

Cooper, M. G. and Smith, L. C.: Satellite Remote Sensing of the Greenland Ice Sheet Ablation Zone: A Review, Remote Sensing, 11(20), 2405, doi:10.3390/rs11202405, 2019.

Cooper, M. G., Smith, L. C., Rennermalm, A. K., Miège, C., Pitcher, L. H., Ryan, J. C., Yang, K. and Cooley, S. W.: Meltwater storage in low-density near-surface bare ice in the Greenland ice sheet ablation zone, The Cryosphere, 12(3), 955–970, doi:10.5194/tc-12-955-2018, 2018.

Dadic, R., Mullen, P. C., Schneebeli, M., Brandt, R. E. and Warren, S. G.: Effects of bubbles, cracks, and volcanic tephra on the spectral albedo of bare ice near the Transantarctic Mountains: Implications for sea glaciers

https://doi.org/10.5194/tc-2020-53
Preprint. Discussion started: 17 March 2020

on Snowball Earth, Journal of Geophysical Research: Earth Surface, 118(3), 1658–1676, doi:10.1002/jgrf.20098, 2013.

Deems, J. S., Painter, T. H. and Finnegan, D. C.: Lidar measurement of snow depth: a review, Journal of Glaciology, 59(215), 467–479, doi:10.3189/2013JoG12J154, 2013.

Fisher, F. N., King, M. D. and Lee-Taylor, J.: Extinction of UV-visible radiation in wet midlatitude (maritime) snow: Implications for increased NOx emission, J. Geophys. Res., 110(D21), D21301, doi:10.1029/2005JD005963, 2005.

France, J. L., King, M. D., Frey, M. M., Erbland, J., Picard, G., Preunkert, S., MacArthur, A. and Savarino, J.: Snow optical properties at Dome C (Concordia), Antarctica; implications for snow emissions and snow chemistry of reactive nitrogen, Atmospheric Chemistry and Physics, 11(18), 9787–9801, doi:https://doi.org/10.5194/acp-11-9787-2011, 2011.

Frey, K. E., Perovich, D. K. and Light, B.: The spatial distribution of solar radiation under a melting Arctic sea ice cover, Geophysical Research Letters, 38(22), doi:10.1029/2011GL049421, 2011.

Gardner, A. S., Smith, B. E., Brunt, K. M., Harding, D. J., Neumann, T. and Walsh, K.: ICESat2 subsurface-scattering biases estimated based on the 2015 SIMPL/AVRIS campaign, in AGU Fall Meeting Abstracts, vol. 41, pp. C41C-0710. [online] Available from: http://adsabs.harvard.edu/abs/2015AGUFM.C41C0710G (Accessed 25 January 2019), 2015.

Gerland, S., Liston, G. E., Winther, J.-G., Ørbæk, J. B. and Ivanov, B. V.: Attenuation of solar radiation in Arctic snow: field observations and modelling, Annals of Glaciology, 31, 364–368, doi:10.3189/172756400781820444, 2000.

Goelles, T. and Bøggild, C. E.: Albedo reduction of ice caused by dust and black carbon accumulation: a model applied to the K-transect, West Greenland, Journal of Glaciology, 63(242), 1063–1076, doi:10.1017/jog.2017.74, 2017.

Goelles, T., Bøggild, C. E. and Greve, R.: Ice sheet mass loss caused by dust and black carbon accumulation, The Cryosphere, 9(5), 1845–1856, doi:10.5194/tc-9-1845-2015, 2015.

Greeley, A., Kurtz, N. T., Neumann, T. and Markus, T.: Estimating Surface Elevation Bias Due to Subsurface Scattered Photons from Visible Wavelength Laser Altimeters, in AGU Fall Meeting Abstracts, vol. 51. [online] Available from: http://adsabs.harvard.edu/abs/2017AGUFM.C51A0961G (Accessed 25 January 2019), 2017.

Grenfell, T. C.: The Effects of Ice Thickness on the Exchange of Solar Radiation Over the Polar Oceans, Journal of Glaciology, 22(87), 305–320, doi:10.3189/S0022143000014295, 1979.

Grenfell, T. C.: A radiative transfer model for sea ice with vertical structure variations, Journal of Geophysical Research: Oceans, 96(C9), 16991–17001, doi:10.1029/91JC01595, 1991.

Grenfell, T. C. and Maykut, G. A.: The Optical Properties of Ice and Snow in the Arctic Basin*, Journal of Glaciology, 18(80), 445–463, doi:10.3189/S0022143000021122, 1977.

https://doi.org/10.5194/tc-2020-53
Preprint. Discussion started: 17 March 2020

Grenfell, T. C. and Perovich, D. K.: Radiation absorption coefficients of polycrystalline ice from 400–1400 nm, J. Geophys. Res., 86(C8), 7447–7450, doi:10.1029/JC086iC08p07447, 1981.

Grenfell, T. C., Light, B. and Perovich, D. K.: Spectral transmission and implications for the partitioning of shortwave radiation in arctic sea ice, Ann. Glaciol., 44, 1–6, doi:10.3189/172756406781811763, 2006.

Hoffman, M. J., Fountain, A. G. and Liston, G. E.: Near-surface internal melting: a substantial mass loss on Antarctic Dry Valley glaciers, Journal of Glaciology, 60(220), 361–374, doi:10.3189/2014JoG13J095, 2014.

Holland, M. M., Bailey, D. A., Briegleb, B. P., Light, B. and Hunke, E.: Improved Sea Ice Shortwave Radiation Physics in CCSM4: The Impact of Melt Ponds and Aerosols on Arctic Sea Ice*, J. Climate, 25(5), 1413–1430, doi:10.1175/JCLI-D-11-00078.1, 2012.

Järvinen, O. and Leppäranta, M.: Solar radiation transfer in the surface snow layer in Dronning Maud Land, Antarctica, Polar Science, 7(1), 1–17, doi:10.1016/j.polar.2013.03.002, 2013.

King, M. D. and Simpson, W. R.: Extinction of UV radiation in Arctic snow at Alert, Canada (82°N), J. Geophys. Res., 106(D12), 12499–12507, doi:10.1029/2001JD900006, 2001.

Kuipers Munneke, P., van den Broeke, M. R., Reijmer, C. H., Helsen, M. M., Boot, W., Schneebeli, M. and Steffen, K.: The role of radiation penetration in the energy budget of the snowpack at Summit, Greenland, The Cryosphere, 3(2), 155–165, doi:10.5194/tc-3-155-2009, 2009.

Light, B., Maykut, G. A. and Grenfell, T. C.: A two-dimensional Monte Carlo model of radiative transfer in sea ice, Journal of Geophysical Research: Oceans, 108(C7), 3219, doi:10.1029/2002JC001513, 2003.

Light, B., Maykut, G. A. and Grenfell, T. C.: A temperature-dependent, structural-optical model of first-year sea ice, J. Geophys. Res., 109(C6), C06013, doi:10.1029/2003JC002164, 2004.

Light, B., Grenfell, T. C. and Perovich, D. K.: Transmission and absorption of solar radiation by Arctic sea ice during the melt season, J. Geophys. Res., 113(C3), C03023, doi:10.1029/2006JC003977, 2008.

Liston, G. E. and Winther, J.-G.: Antarctic Surface and Subsurface Snow and Ice Melt Fluxes, J. Climate, 18(10), 1469–1481, doi:10.1175/JCLI3344.1, 2005.

Liston, G. E., Bruland, O., Elvehøy, H. and Sand, K.: Below-surface ice melt on the coastal Antarctic ice sheet, Journal of Glaciology, 45(150), 273–285, doi:10.3189/002214399793377130, 1999a.

Liston, G. E., Bruland, O., Winther, J.-G., Elvehøy, H. and Sand, K.: Meltwater production in Antarctic blue-ice areas: sensitivity to changes in atmospheric forcing, Polar Research, 18(2), 283–290, doi:10.1111/j.1751-8369.1999.tb00305.x, 1999b.

Markus, T., Neumann, T., Martino, A., Abdalati, W., Brunt, K., Csatho, B., Farrell, S., Fricker, H., Gardner, A., Harding, D., Jasinski, M., Kwok, R., Magruder, L., Lubin, D., Luthcke, S., Morison, J., Nelson, R., Neuenschwander, A., Palm, S., Popescu, S., Shum, C., Schutz, B. E., Smith, B., Yang, Y. and Zwally, J.: The Ice,

https://doi.org/10.5194/tc-2020-53
Preprint. Discussion started: 17 March 2020

Cloud, and land Elevation Satellite-2 (ICESat-2): Science requirements, concept, and implementation, Remote Sensing of Environment, 190, 260–273, doi:10.1016/j.rse.2016.12.029, 2017.

Mätzler, C.: MATLAB Functions for Mie Scattering and Absorption Version 2, Research Report, Institut für Angewandte Physik, Bern, Switzerland., 2002.

Meirold-Mautner, I. and Lehning, M.: Measurements and model calculations of the solar shortwave fluxes in snow on Summit, Greenland, Annals of Glaciology, 38, 279–284, doi:10.3189/172756404781814753, 2004.

Mullen, P. C. and Warren, S. G.: Theory of the optical properties of lake ice, J. Geophys. Res., 93(D7), 8403–8414, doi:10.1029/JD093iD07p08403, 1988.

Müller, F. and Keeler, C. M.: Errors in Short-Term Ablation Measurements on Melting Ice Surfaces, Journal of Glaciology, 8(52), 91–105, doi:10.3189/S0022143000020785, 1969.

Pegau, W. S. and Zaneveld, J. R. V.: Field measurements of in-ice radiance, Cold Regions Science and Technology, 31(1), 33–46, doi:10.1016/S0165-232X(00)00004-5, 2000.

Perovich, D. K.: The Optical Properties of Sea Ice., U.S. Army Cold Regions Research and Engineering Laboratory, Hanover, NH., 1996.

Perovich, D. K. and Govoni, J. W.: Absorption coefficients of ice from 250 to 400 nm, Geophys. Res. Lett., 18(7), 1233–1235, doi:10.1029/91GL01642, 1991.

Picard, G., Libois, Q. and Arnaud, L.: Refinement of the ice absorption spectrum in the visible using radiance profile measurements in Antarctic snow, The Cryosphere, 10(6), 2655–2672, doi:10.5194/tc-10-2655-2016, 2016.

Price, P. B. and Bergström, L.: Optical properties of deep ice at the South Pole: scattering, Appl. Opt., AO, 36(18), 4181–4194, doi:10.1364/AO.36.004181, 1997.

Ridley, J. K. and Partington, K. C.: A model of satellite radar altimeter return from ice sheets, International Journal of Remote Sensing, 9(4), 601–624, doi:10.1080/01431168808954881, 1988.

Rignot, E., Echelmeyer, K. and Krabill, W.: Penetration depth of interferometric synthetic-aperture radar signals in snow and ice, Geophysical Research Letters, 28(18), 3501–3504, doi:10.1029/2000GL012484, 2001.

Ryan, J. C., Hubbard, A. L., Stibal, M., Irvine-Fynn, T. D., Cook, J., Smith, L. C., Cameron, K. and Box, J. E.: Dark zone of the Greenland Ice Sheet controlled by distributed biologically-active impurities, Nature Communications, 9(1), 1065, doi:10.1038/s41467-018-03353-2, 2018.

Schuster, A.: Radiation through a foggy atmosphere, The Astrophysical Journal, XX1(1), 1–22, 1905.

Schuster, C.: Weathering crust processes on melting glacier ice (Alberta, Canada), Theses and Dissertations (Comprehensive) [online] Available from: http://scholars.wlu.ca/etd/489, 2001.

https://doi.org/10.5194/tc-2020-53
Preprint. Discussion started: 17 March 2020

Schutz, B. E., Zwally, H. J., Shuman, C. A., Hancock, D. and DiMarzio, J. P.: Overview of the ICESat Mission, Geophys. Res. Lett., 32(21), L21S01, doi:10.1029/2005GL024009, 2005.

Stibal, M., Box, J. E., Cameron, K. A., Langen, P. L., Yallop, M. L., Mottram, R. H., Khan, A. L., Molotch, N. P., Chrismas, N. A. M., Quaglia, F. C., Remias, D., Smeets, C. J. P. P., Broeke, M. R. van den, Ryan, J. C., Hubbard, A., Tranter, M., As, D. van and Ahlstrøm, A. P.: Algae Drive Enhanced Darkening of Bare Ice on the Greenland Ice Sheet, Geophysical Research Letters, 44(22), 11,463-11,471, doi:10.1002/2017GL075958, 2017.

Takeuchi, N.: Optical characteristics of cryoconite (surface dust) on glaciers: the relationship between light absorbency and the property of organic matter contained in the cryoconite, Annals of Glaciology, 34(1), 409–414, doi:10.3189/172756402781817743, 2002.

Tedstone, A. J., Bamber, J. L., Cook, J. M., Williamson, C. J., Fettweis, X., Hodson, A. J. and Tranter, M.: Dark ice dynamics of the south-west Greenland Ice Sheet, The Cryosphere, 11(6), 2491–2506, doi:10.5194/tc-11-2491-2017, 2017.

Tuzet, F., Dumont, M., Arnaud, L., Voisin, D., Lamare, M., Larue, F., Revuelto, J. and Picard, G.: Influence of light-absorbing particles on snow spectral irradiance profiles, The Cryosphere, 13(8), 2169–2187, doi:10.5194/tc-13-2169-2019, 2019.

Warren, S. G.: Optical properties of snow, Rev. Geophys., 20(1), 67–89, doi:10.1029/RG020i001p00067, 1982.

Warren, S. G.: Optical constants of ice from the ultraviolet to the microwave, Appl. Opt., AO, 23(8), 1206–1225, doi:10.1364/AO.23.001206, 1984.

Warren, S. G. and Brandt, R. E.: Optical constants of ice from the ultraviolet to the microwave: A revised compilation, J. Geophys. Res., 113(D14), D14220, doi:10.1029/2007JD009744, 2008.

Warren, S. G., Brandt, R. E., Grenfell, T. C. and McKay, C. P.: Snowball Earth: Ice thickness on the tropical ocean, Journal of Geophysical Research: Oceans, 107(C10), 31-1-31–18, doi:10.1029/2001JC001123, 2002.

Warren, S. G., Brandt, R. E. and Grenfell, T. C.: Visible and near-ultraviolet absorption spectrum of ice from transmission of solar radiation into snow, Appl. Opt., AO, 45(21), 5320–5334, doi:10.1364/AO.45.005320, 2006.

Yallop, M. L., Anesio, A. M., Perkins, R. G., Cook, J., Telling, J., Fagan, D., MacFarlane, J., Stibal, M., Barker, G., Bellas, C., Hodson, A., Tranter, M., Wadham, J. and Roberts, N. W.: Photophysiology and albedo-changing potential of the ice algal community on the surface of the Greenland ice sheet, ISME J, 6(12), 2302–2313, doi:10.1038/ismej.2012.107, 2012.

Yang, Y., Marshak, A., Han, M., Palm, S. P. and Harding, D. J.: Snow grain size retrieval over the polar ice sheets with the Ice, Cloud, and land Elevation Satellite (ICESat) observations, Journal of Quantitative Spectroscopy and Radiative Transfer, 188, 159–164, doi:10.1016/j.jqsrt.2016.03.033, 2017.

Zebker, H. A. and Weber Hoen, E.: Penetration depths inferred from interferometric volume decorrelation observed over the Greenland Ice Sheet, IEEE Transactions on Geoscience and Remote Sensing, 38(6), 2571–2583, doi:10.1109/36.885204, 2000.

https://doi.org/10.5194/tc-2020-53
Preprint. Discussion started: 17 March 2020

The Cryosphere
Discussions
Open Access
EGU

Figures

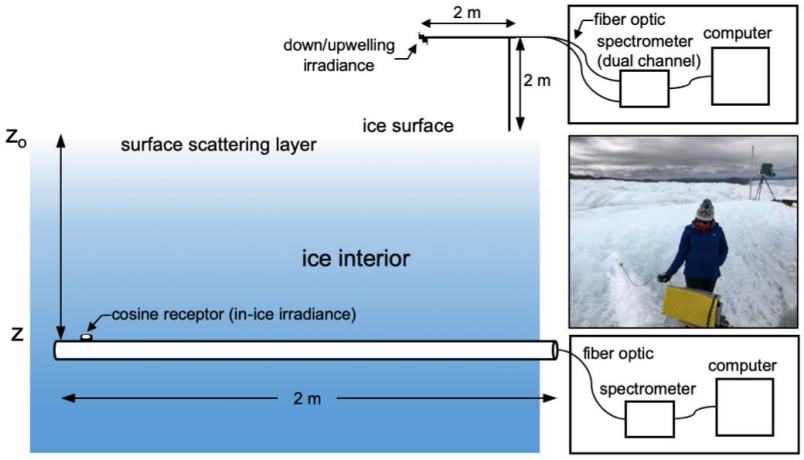

Figure 1: Experimental setup schematic. The horizontal cylindrical rod is an insulated white PVC tube of 2 m length. Holes are drilled level and horizontal into the ice, the tube is inserted, and drill shavings are packed around the hole to prevent stray reflections, working from the bottom toward the top. Inside the tube is a fiber optic cable attached to a remote cosine receptor with a Spectralon diffusing element oriented parallel to the rod (normal to the vertical), set approximately 2 mm out from the tube exterior and in contact with the overlying ice. The cosine receptor collects the downwelling light, guides it to the fiber optic cable that transmits the light to an Ocean Optics JAZ spectrometer, and a computer running the Ocean Optics Ocean View software records the spectra. Background upwelling and downwelling surface spectra are recorded on a 2 m mast drilled into the ice approximately 3 m to the northwest of the in-ice measurement location (visible in the photo). After all measurements are complete, a 2 m ruler is inserted into each hole, two at a time, and the distance between the holes is recorded to determine their depth relative to each other and to the surface.

https://doi.org/10.5194/tc-2020-53
Preprint. Discussion started: 17 March 2020

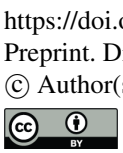

The Cryosphere Discussions
Open Access
EGU

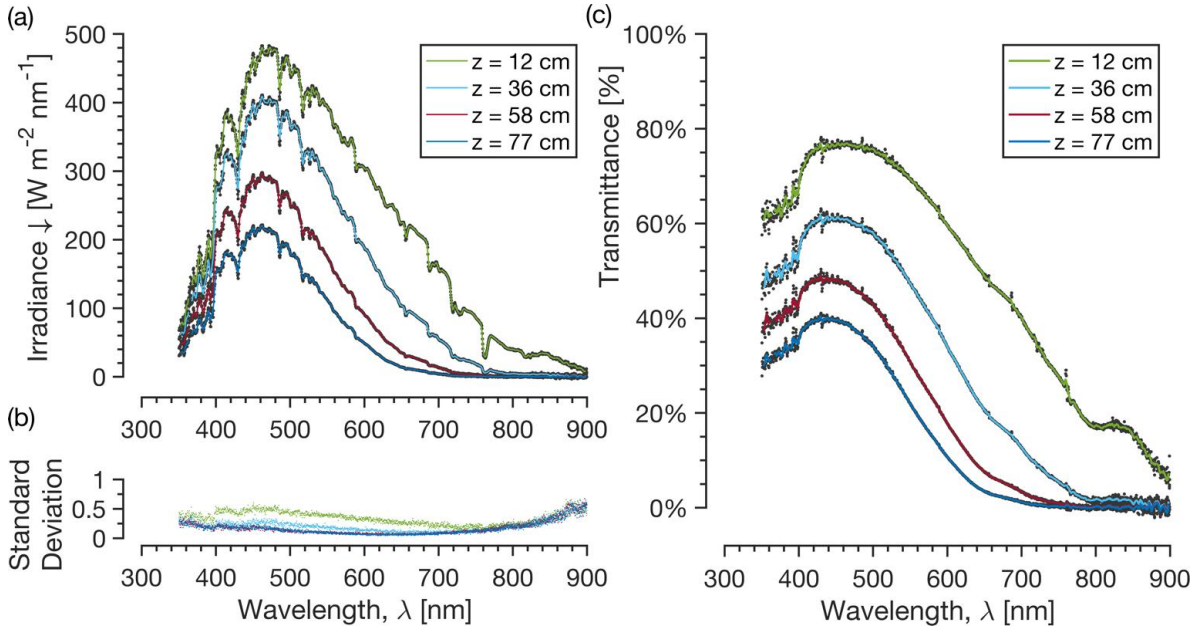

Figure 2: (a) Field spectra of in-ice irradiance at four depths below the ice surface collected on 20 July 2018 between 13:45 and 14:35 local time in the western Greenland Ice Sheet ablation zone (67.15 °N, 50.02 °W). Raw data were recorded at 1 Hz frequency for 30 seconds, yielding 30 irradiance profiles at each depth. Shown here are 30-second averages at ~0.35 nm spectral resolution for each depth (black dots), and 1-nm interpolated values smoothed with a 3-nm centered moving mean filter for clarity (continuous lines). (b) Standard deviation of the 1 Hz raw data (N=30 for each value) is <1 W m^{-2} nm^{-1} at all wavelengths and measured depths. (c) Relative irradiance (in-ice irradiance divided by surface downwelling irradiance) at each depth, with 30-second averages (black dots) and 1-nm interpolated values (continuous lines) as in (a).

https://doi.org/10.5194/tc-2020-53
Preprint. Discussion started: 17 March 2020

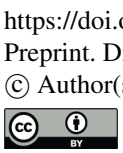

The Cryosphere Discussions
Open Access
EGU

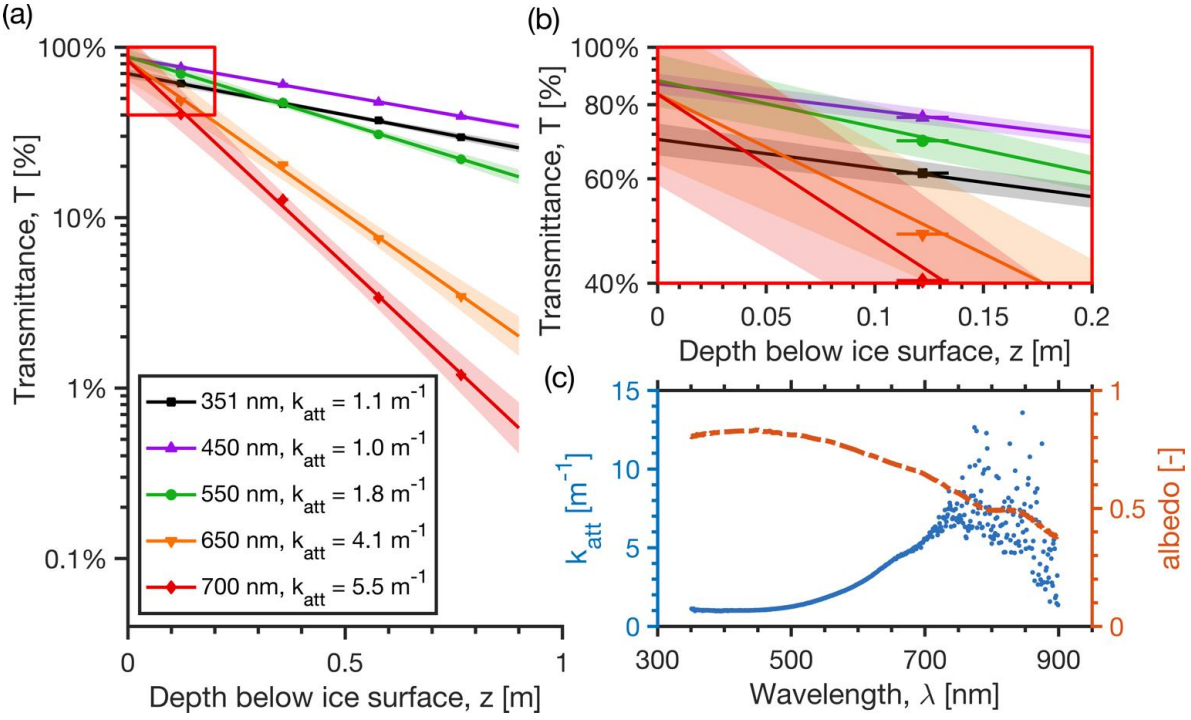

Figure 3: (a) Sample least-squares regressions between measured transmittance (indicated by solid symbols) and depth for five representative wavelengths spanning the measured spectral range. The slope of each line is the attenuation coefficient k_{att} (k_{att} values are indicated in the legend). Shaded bounds are one standard error in the linear regression estimate. (b) Red box inset in (a) shows the y-axis intercept of each regression is less than 100%, indicating the magnitude of deviation from Bouguer's law. Horizontal lines through each symbol represent ±1.2 cm vertical measurement uncertainty. (c) Spectral k_{att} (blue dots; left axis) and spectral albedo (red dashed line; right axis). Beyond ~700 nm, in-ice transmitted irradiance is too low to reliably estimate k_{att} (see Figure 2a and 2c), as indicated by the increased scatter in k_{att} values. The minimum k_{att} value within the range 350–700 nm is 0.96 m^{-1} (0.87 m^{-1} in solid ice-equivalent units) and occurs at 396 nm. The maximum albedo value is 0.83 and occurs at 447 nm.

https://doi.org/10.5194/tc-2020-53
Preprint. Discussion started: 17 March 2020

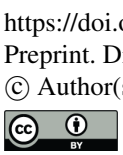

The Cryosphere Discussions
Open Access
EGU

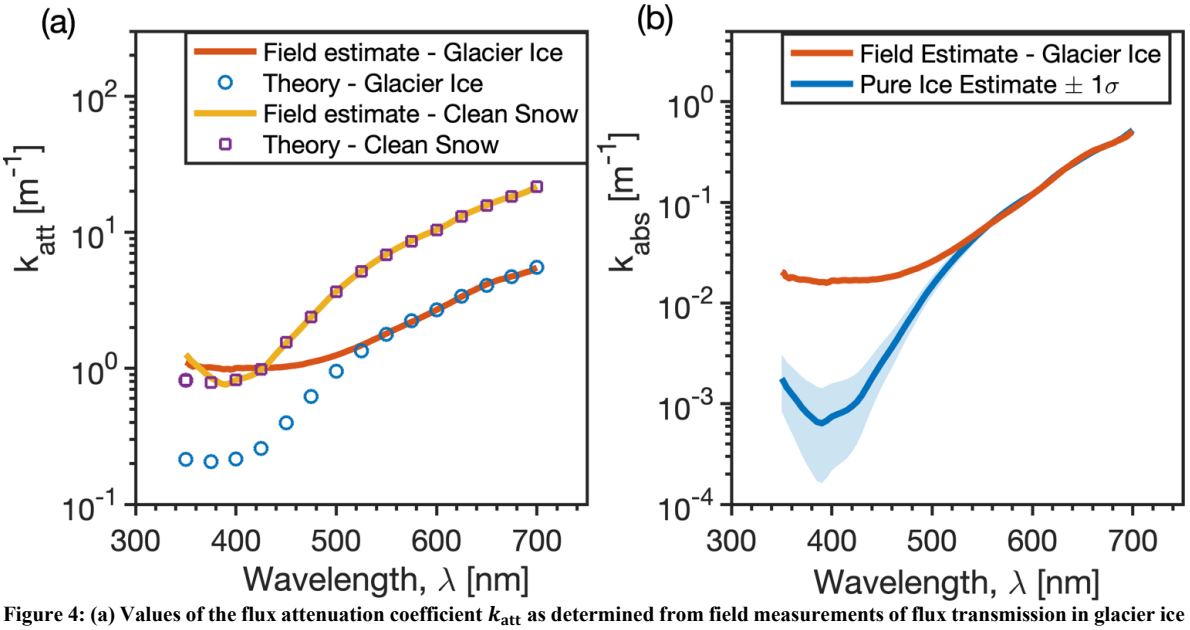

Figure 4: (a) Values of the flux attenuation coefficient k_{att} as determined from field measurements of flux transmission in glacier ice (this study), theoretical values for glacier ice using two-stream theory, field measurements in clean snow (Warren et al., 2006), and theoretical values for snow using two-stream theory. The theoretical k_{att} values for ice and snow differ by a constant offset proportional to the ratio of their optical grain sizes, whereas the field-estimate for glacier ice diverges from theory in the region 350–525 nm. (b) Flux absorption coefficient, k_{abs} estimated from the field-estimated k_{att} values using the method of Warren et al (2006) compared to flux absorption coefficient for pure ice, $k_{abs,ice}$ obtained from field measurements in clean snow in Antarctica by Warren et al (2006). Uncertainty ($\pm$ one standard error in the linear regression coefficient) are shown for both estimates but are imperceptible for glacier ice. As with k_{att}, the k_{abs} values are up to one order of magnitude larger at $\lambda < 525$ nm for glacier ice than pure ice, suggesting light absorbing particles enhance flux absorption at our field site.

https://doi.org/10.5194/tc-2020-53
Preprint. Discussion started: 17 March 2020

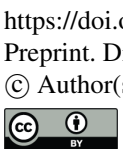

The Cryosphere Discussions
Open Access
EGU

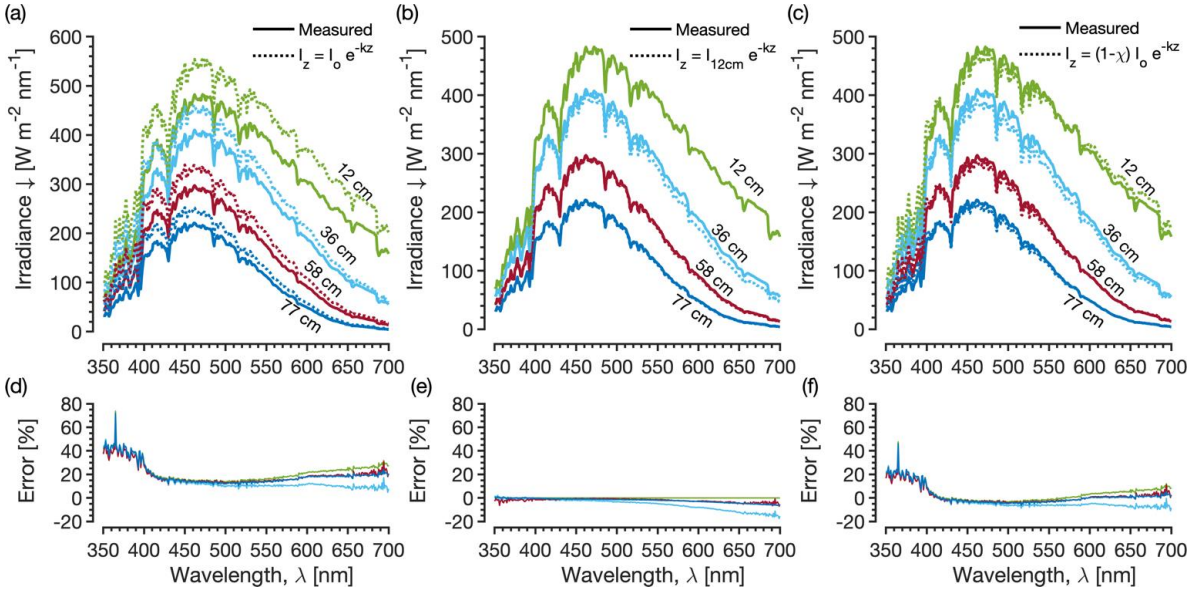

Figure 5: Measured in-ice irradiance compared with three empirical models of in-ice irradiance: (a) Bouguer's law (Eq. 2) with no modification, (b) Bouguer's law (Eq. 2) with $I(z_0) = I(z_{12cm})$, which effectively removes errors due to attenuation in the 0–12 cm near-surface region and isolates the accuracy of Bouguer's law within the ice interior, and (c) the modified Bouguer law (Eq. 7) with $\chi = 15\%$. The error structure (d–f) provides insight into the attenuation processes in the 0–12 cm region: (d) relative errors (%) are positive (model under-predicts attenuation) at all wavelengths but are highest in the near-UV, lowest in the blue, and increase monotonically into the red end of the visible spectrum. The spectral dependence suggests a contribution of absorption to near-surface attenuation enhancement; (e) errors are negative (model over-predicts attenuation) and generally decrease monotonically with increasing wavelength from the near-UV through the blue-green; (f) as in (d) the spectral pattern of error due to near-surface attenuation is preserved, but errors are much lower due to the χ parameter. Taken together, near-surface attenuation enhancement is on the order 5–50% but has less relative influence in the blue-green spectrum and more relative influence in the red-orange and near-UV and violet regions of the visible spectrum.

https://doi.org/10.5194/tc-2020-53
Preprint. Discussion started: 17 March 2020

The Cryosphere
Discussions
Open Access
EGU

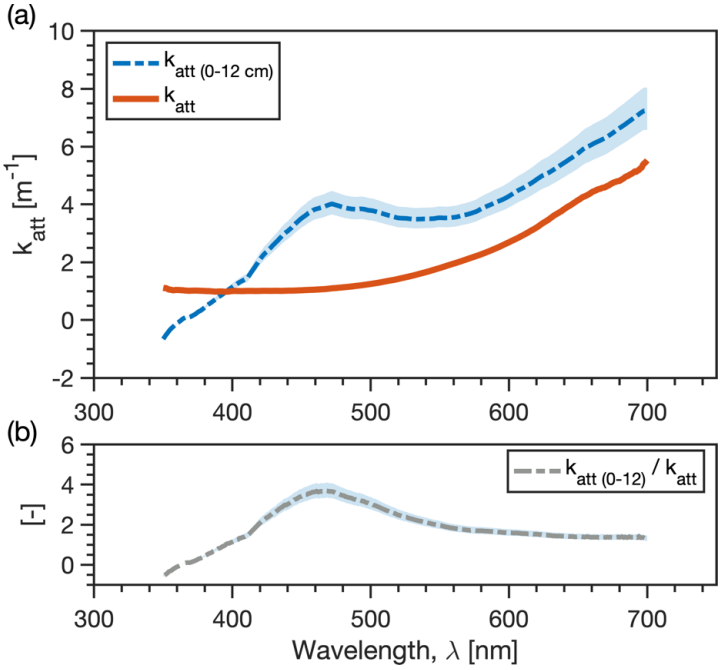

Figure 6: (a) Effective attenuation coefficient k_{att} for the near-surface 0–12 cm region estimated with a finite-difference solution to Eq. (1) compared to k_{att} values estimated for the interior 12–77 cm region. The shaded bounds represent ±1.2 cm vertical measurement uncertainty. (b) Effective k_{att} values are ~1.6× higher at wavelengths larger than about 600 nm but are ~3.7× higher between 400–600 nm. The shaded bounds represent ±1.2 cm vertical measurement uncertainty. The spectral dependence suggests higher influence of absorptive impurities on attenuation enhancement near the ice surface than in the ice interior. In contrast, the relatively constant attenuation enhancement beyond about 600 nm suggests near-surface ice microstructure, for example the size, shape, and orientation of weathered ice grains or air bubbles, contributes to enhanced near-surface attenuation.

https://doi.org/10.5194/tc-2020-53
Preprint. Discussion started: 17 March 2020

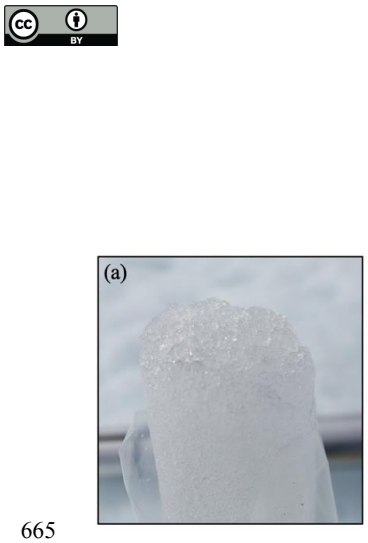

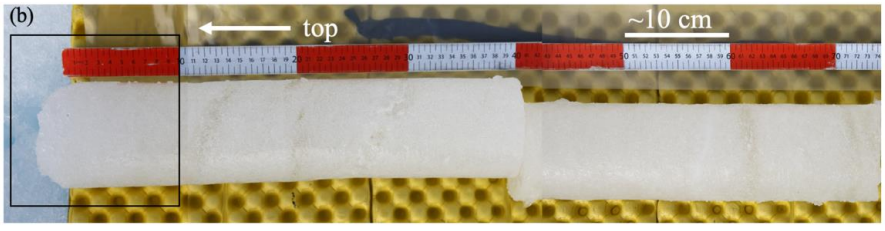

665 **Figure 7: Photographs of an ice core collected at the field site. (a) The upper few centimetres of ice is semi-granular. (b) The 122 cm ice core was broken into three segments corresponding to depths of 4–45 cm, 45–74 cm, and 74–122 cm below the ice surface (the far right of the image in (b) is at 74 cm). The density of these segments is 801 kg m^{-3}, 884 kg m^{-3}, and 888 kg m^{-3}, respectively. Black box in (b) is approximately the image area in (a).**

https://doi.org/10.5194/tc-2020-53
Preprint. Discussion started: 17 March 2020

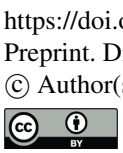

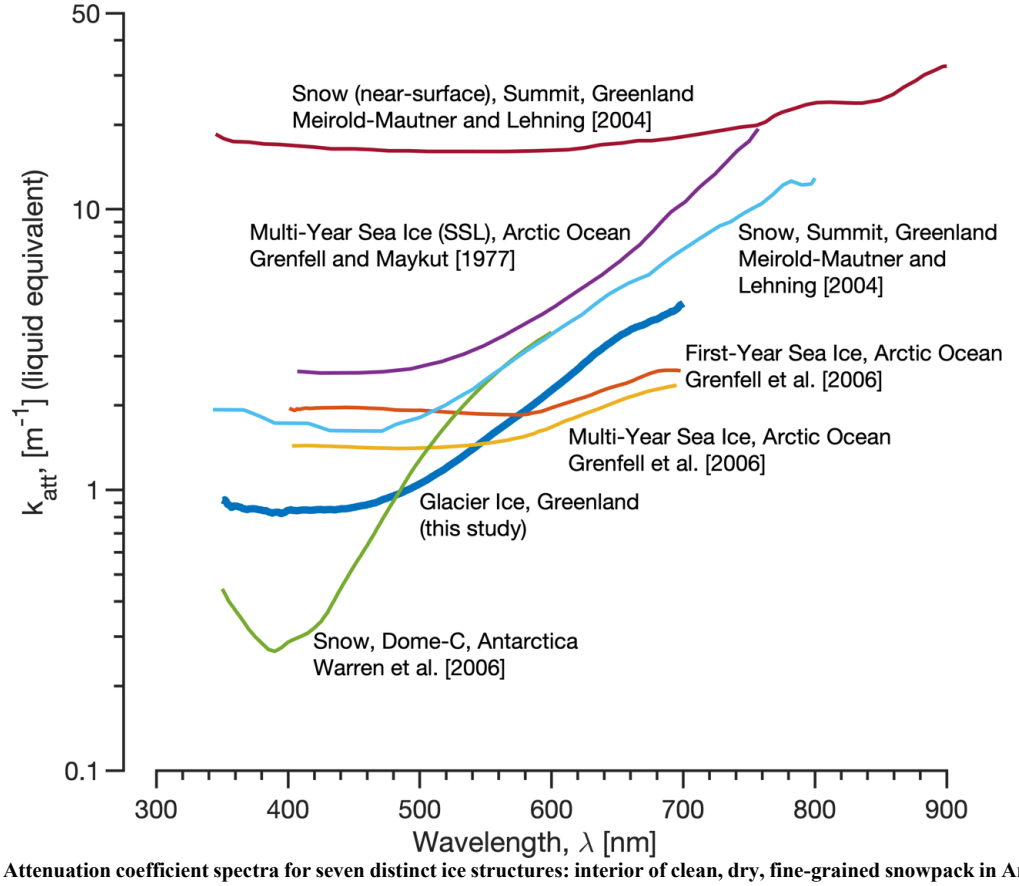

Figure 8: Attenuation coefficient spectra for seven distinct ice structures: interior of clean, dry, fine-grained snowpack in Antarctica (Warren et al., 2006), interior of ablating glacier ice in Greenland (this study), interior of multi-year sea ice in the Arctic Ocean (Grenfell et al., 2006), interior of first-year sea ice in the Arctic Ocean (Grenfell et al., 2006), interior of dry, fine-grained snow near Summit, Greenland (Meirold-Mautner and Lehning, 2004), surface scattering layer (SSL) of multi-year sea ice in the Arctic Ocean (Grenfell and Maykut, 1977), and near-surface (5 cm depth) dry, fine-grained snow near Summit, Greenland (analogous to SSL) (Meirold-Mautner and Lehning, 2004). Differences in attenuation magnitude at each wavelength are mostly controlled by structural differences that control scattering, whereas spectral differences are mostly controlled by differences in type and concentration of absorbing impurities. In general, glacial ice attenuates light less efficiently than all other examples shown, with the exception of clean snow near Dome-C in Antarctica for $\lambda < 450$ nm, and multi-year and first-year sea ice for $\lambda > 600$ nm.

https://doi.org/10.5194/tc-2020-53
Preprint. Discussion started: 17 March 2020

The Cryosphere Discussions
Open Access
EGU

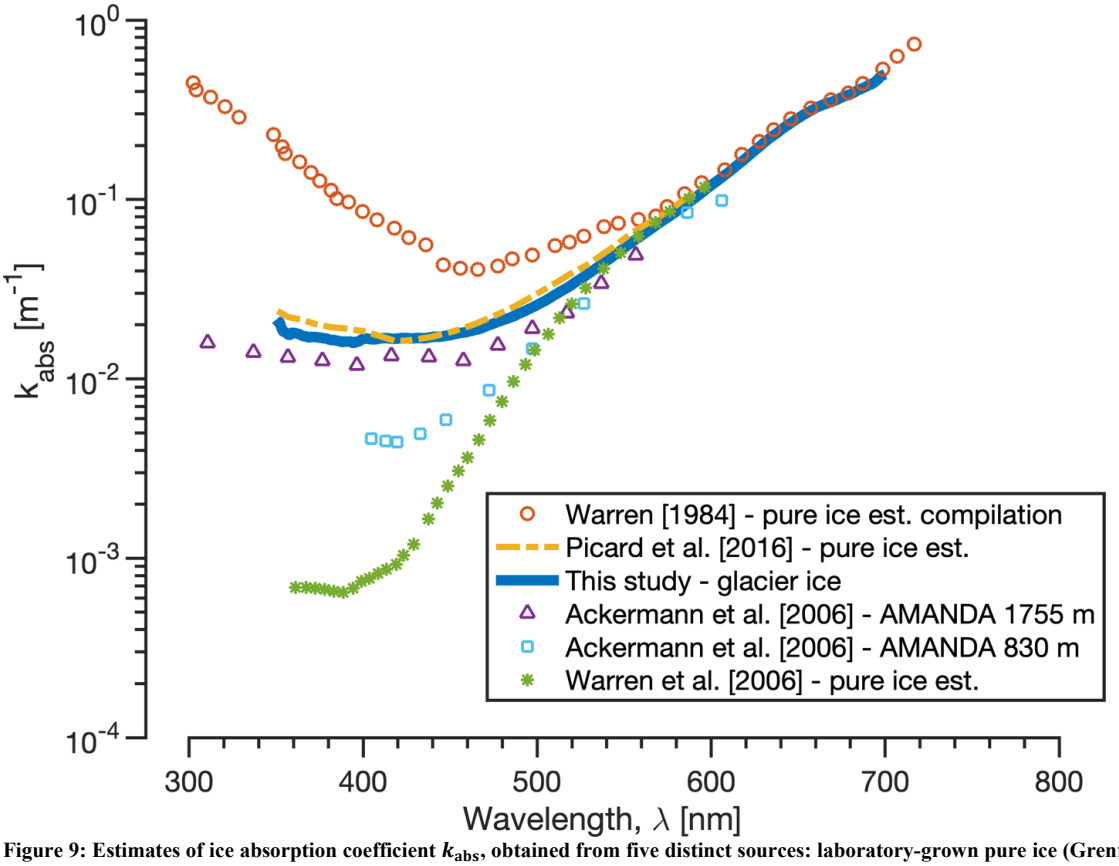

680 **Figure 9: Estimates of ice absorption coefficient k_{abs}, obtained from five distinct sources: laboratory-grown pure ice (Grenfell and Perovich, 1981; Perovich and Govoni, 1991), as compiled in Warren (1984), snow in Antarctica, with the effect of light absorbing particles (LAPs) removed (pure ice estimate) (Picard et al., 2016), glacial ice in Greenland with unknown concentration of LAPs (this study), compressed glacier ice at 1755 m depth and 830 m depth in the Antarctic Ice Sheet contaminated by dust deposited**
685 **during the late Pleistocene and Early Holocene, respectively (Ackermann et al., 2006), and snow in Antarctica with the effect of LAPs removed (pure ice estimate) (Warren et al., 2006). The Picard *et al* (2016) pure ice estimate is higher at some wavelengths than our glacier ice estimate, which was undoubtedly influenced by LAPs, providing support for the pure ice estimate from Warren *et al* (2006).**

https://doi.org/10.5194/tc-2020-53
Preprint. Discussion started: 17 March 2020

The Cryosphere Discussions
Open Access
EGU

690 **Appendix 1**

Table A1: Estimates of attenuation coefficient, absorption coefficient, and scattering coefficient obtained from solar flux transmission measurements in glacier ice. Coefficient values are in units of solid ice-equivalent referenced to in-situ measured ice density 835 kg m^3. Also given are values for one standard error in the linear regression coefficient and the coefficient of determination (r^2) for k_{att}, and one standard error in the k_{abs} estimate.

wavelength (nm)	k_{att} (m^{-1})	standard error (k_{att})	r^2	k_{abs} (m^{-1})	standard error (k_{abs})	k_{sca} (m^{-1})
350	1.049	0.043	0.998	0.0222	-0.00064	1.036
351	1.013	0.028	0.999	0.0204	-0.00059	0.992
352	0.978	0.013	1.000	0.0186	-0.00054	0.947
353	0.979	0.043	0.997	0.0191	-0.00055	0.960
354	1.022	0.041	0.997	0.0202	-0.00059	0.987
355	0.936	0.027	0.999	0.0181	-0.00052	0.935
356	0.892	0.085	0.985	0.0159	-0.00046	0.878
357	0.959	0.037	0.998	0.0179	-0.00052	0.930
358	0.937	0.030	0.998	0.0178	-0.00052	0.928
359	0.960	0.010	1.000	0.0184	-0.00053	0.943
360	0.948	0.046	0.996	0.0179	-0.00052	0.930
361	0.938	0.056	0.994	0.0183	-0.00053	0.941
362	0.946	0.030	0.998	0.0179	-0.00052	0.929
363	0.943	0.029	0.998	0.0175	-0.00051	0.921
364	0.940	0.022	0.999	0.0175	-0.00051	0.921
365	0.937	0.024	0.999	0.0175	-0.00051	0.920
366	0.934	0.025	0.999	0.0175	-0.00051	0.919
367	0.908	0.011	1.000	0.0167	-0.00048	0.899
368	0.921	0.031	0.998	0.0169	-0.00049	0.906
369	0.934	0.011	1.000	0.0175	-0.00051	0.920
370	0.916	0.024	0.999	0.0169	-0.00049	0.904
371	0.922	0.011	1.000	0.0170	-0.00049	0.908
372	0.931	0.027	0.999	0.0174	-0.00050	0.916
373	0.925	0.018	0.999	0.0169	-0.00049	0.904

https://doi.org/10.5194/tc-2020-53
Preprint. Discussion started: 17 March 2020

374	0.935	0.017	0.999	0.0174	-0.00050	0.918
375	0.921	0.018	0.999	0.0167	-0.00048	0.900
376	0.921	0.023	0.999	0.0167	-0.00048	0.900
377	0.924	0.022	0.999	0.0170	-0.00049	0.908
378	0.919	0.022	0.999	0.0168	-0.00049	0.902
379	0.923	0.025	0.999	0.0169	-0.00049	0.905
380	0.910	0.017	0.999	0.0165	-0.00048	0.893
381	0.918	0.018	0.999	0.0167	-0.00048	0.900
382	0.914	0.013	1.000	0.0162	-0.00047	0.885
383	0.900	0.011	1.000	0.0162	-0.00047	0.887
384	0.912	0.020	0.999	0.0164	-0.00048	0.892
385	0.921	0.022	0.999	0.0169	-0.00049	0.905
386	0.893	0.030	0.998	0.0160	-0.00046	0.881
387	0.894	0.040	0.997	0.0160	-0.00046	0.881
388	0.880	0.033	0.998	0.0157	-0.00045	0.872
389	0.905	0.020	0.999	0.0163	-0.00047	0.889
390	0.897	0.013	1.000	0.0161	-0.00047	0.883
391	0.914	0.014	1.000	0.0166	-0.00048	0.897
392	0.904	0.024	0.999	0.0160	-0.00046	0.881
393	0.882	0.016	0.999	0.0155	-0.00045	0.867
394	0.906	0.015	1.000	0.0165	-0.00048	0.893
395	0.895	0.012	1.000	0.0160	-0.00046	0.880
396	0.876	0.032	0.998	0.0153	-0.00044	0.862
397	0.893	0.012	1.000	0.0161	-0.00047	0.882
398	0.915	0.004	1.000	0.0167	-0.00048	0.900
399	0.904	0.012	1.000	0.0164	-0.00047	0.890
400	0.919	0.016	0.999	0.0167	-0.00048	0.900
401	0.923	0.015	1.000	0.0171	-0.00049	0.909
402	0.911	0.015	1.000	0.0166	-0.00048	0.895
403	0.920	0.015	1.000	0.0168	-0.00049	0.902
404	0.926	0.017	0.999	0.0169	-0.00049	0.903
405	0.896	0.012	1.000	0.0162	-0.00047	0.885
406	0.917	0.016	1.000	0.0168	-0.00049	0.901

https://doi.org/10.5194/tc-2020-53
Preprint. Discussion started: 17 March 2020

407	0.909	0.016	0.999	0.0164	-0.00048	0.892
408	0.914	0.016	0.999	0.0167	-0.00048	0.899
409	0.920	0.019	0.999	0.0169	-0.00049	0.905
410	0.911	0.016	0.999	0.0167	-0.00048	0.898
411	0.918	0.009	1.000	0.0169	-0.00049	0.904
412	0.924	0.018	0.999	0.0170	-0.00049	0.908
413	0.915	0.011	1.000	0.0167	-0.00048	0.900
414	0.918	0.006	1.000	0.0170	-0.00049	0.908
415	0.914	0.011	1.000	0.0167	-0.00048	0.898
416	0.919	0.013	1.000	0.0169	-0.00049	0.904
417	0.914	0.016	1.000	0.0166	-0.00048	0.896
418	0.915	0.016	0.999	0.0167	-0.00048	0.900
419	0.913	0.015	1.000	0.0166	-0.00048	0.898
420	0.919	0.013	1.000	0.0169	-0.00049	0.905
421	0.921	0.017	0.999	0.0169	-0.00049	0.904
422	0.916	0.013	1.000	0.0167	-0.00048	0.900
423	0.924	0.010	1.000	0.0170	-0.00049	0.906
424	0.922	0.016	1.000	0.0170	-0.00049	0.907
425	0.917	0.024	0.999	0.0167	-0.00049	0.900
426	0.925	0.017	0.999	0.0171	-0.00049	0.909
427	0.917	0.016	1.000	0.0167	-0.00048	0.899
428	0.917	0.014	1.000	0.0167	-0.00048	0.899
429	0.914	0.015	1.000	0.0167	-0.00048	0.899
430	0.920	0.021	0.999	0.0169	-0.00049	0.903
431	0.929	0.011	1.000	0.0172	-0.00050	0.912
432	0.921	0.014	1.000	0.0169	-0.00049	0.904
433	0.918	0.012	1.000	0.0168	-0.00049	0.902
434	0.917	0.009	1.000	0.0167	-0.00048	0.900
435	0.918	0.017	0.999	0.0168	-0.00049	0.903
436	0.924	0.017	0.999	0.0171	-0.00049	0.909
437	0.916	0.020	0.999	0.0167	-0.00049	0.900
438	0.916	0.021	0.999	0.0169	-0.00049	0.904
439	0.930	0.013	1.000	0.0173	-0.00050	0.914

https://doi.org/10.5194/tc-2020-53
Preprint. Discussion started: 17 March 2020

440	0.926	0.017	0.999	0.0171	-0.00050	0.910
441	0.929	0.014	1.000	0.0173	-0.00050	0.914
442	0.926	0.021	0.999	0.0171	-0.00050	0.910
443	0.923	0.015	1.000	0.0170	-0.00049	0.908
444	0.928	0.016	0.999	0.0172	-0.00050	0.911
445	0.924	0.020	0.999	0.0172	-0.00050	0.913
446	0.933	0.015	1.000	0.0174	-0.00050	0.917
447	0.932	0.015	1.000	0.0174	-0.00050	0.917
448	0.933	0.018	0.999	0.0173	-0.00050	0.915
449	0.932	0.018	0.999	0.0174	-0.00050	0.917
450	0.942	0.018	0.999	0.0177	-0.00051	0.925
451	0.941	0.019	0.999	0.0176	-0.00051	0.923
452	0.939	0.020	0.999	0.0175	-0.00051	0.921
453	0.941	0.017	0.999	0.0177	-0.00051	0.926
454	0.951	0.019	0.999	0.0181	-0.00052	0.934
455	0.948	0.021	0.999	0.0179	-0.00052	0.931
456	0.951	0.022	0.999	0.0180	-0.00052	0.933
457	0.950	0.015	1.000	0.0181	-0.00052	0.935
458	0.951	0.017	0.999	0.0181	-0.00052	0.935
459	0.958	0.017	0.999	0.0183	-0.00053	0.942
460	0.956	0.016	1.000	0.0183	-0.00053	0.940
461	0.952	0.018	0.999	0.0181	-0.00053	0.936
462	0.968	0.018	0.999	0.0187	-0.00054	0.951
463	0.968	0.018	0.999	0.0187	-0.00054	0.949
464	0.964	0.019	0.999	0.0186	-0.00054	0.948
465	0.971	0.019	0.999	0.0188	-0.00055	0.954
466	0.971	0.021	0.999	0.0188	-0.00055	0.954
467	0.979	0.018	0.999	0.0191	-0.00055	0.959
468	0.975	0.022	0.999	0.0190	-0.00055	0.959
469	0.982	0.023	0.999	0.0193	-0.00056	0.965
470	0.993	0.020	0.999	0.0196	-0.00057	0.973
471	0.996	0.021	0.999	0.0196	-0.00057	0.974
472	1.001	0.018	0.999	0.0199	-0.00058	0.981

https://doi.org/10.5194/tc-2020-53
Preprint. Discussion started: 17 March 2020


The Cryosphere Discussions
Open Access
EGU

473	1.001	0.020	0.999	0.0200	-0.00058	0.983
474	1.005	0.024	0.999	0.0202	-0.00058	0.987
475	1.011	0.023	0.999	0.0204	-0.00059	0.991
476	1.012	0.022	0.999	0.0205	-0.00059	0.993
477	1.019	0.024	0.999	0.0207	-0.00060	1.000
478	1.023	0.025	0.999	0.0209	-0.00061	1.004
479	1.027	0.024	0.999	0.0212	-0.00061	1.010
480	1.029	0.023	0.999	0.0211	-0.00061	1.010
481	1.030	0.024	0.999	0.0212	-0.00061	1.011
482	1.041	0.027	0.999	0.0216	-0.00063	1.021
483	1.042	0.024	0.999	0.0218	-0.00063	1.025
484	1.048	0.028	0.999	0.0220	-0.00064	1.029
485	1.049	0.027	0.999	0.0220	-0.00064	1.029
486	1.051	0.022	0.999	0.0220	-0.00064	1.030
487	1.061	0.024	0.999	0.0225	-0.00065	1.040
488	1.069	0.026	0.999	0.0228	-0.00066	1.048
489	1.072	0.027	0.999	0.0229	-0.00066	1.051
490	1.079	0.026	0.999	0.0233	-0.00067	1.058
491	1.087	0.029	0.999	0.0235	-0.00068	1.064
492	1.083	0.026	0.999	0.0235	-0.00068	1.064
493	1.093	0.026	0.999	0.0239	-0.00069	1.072
494	1.102	0.030	0.999	0.0243	-0.00070	1.080
495	1.100	0.035	0.998	0.0243	-0.00070	1.081
496	1.115	0.032	0.999	0.0248	-0.00072	1.091
497	1.119	0.032	0.999	0.0250	-0.00072	1.096
498	1.122	0.032	0.999	0.0251	-0.00073	1.099
499	1.132	0.032	0.999	0.0255	-0.00074	1.107
500	1.134	0.034	0.998	0.0257	-0.00075	1.112
501	1.142	0.030	0.999	0.0261	-0.00076	1.119
502	1.154	0.030	0.999	0.0266	-0.00077	1.130
503	1.157	0.032	0.999	0.0267	-0.00077	1.131
504	1.161	0.032	0.999	0.0271	-0.00078	1.139
505	1.171	0.032	0.999	0.0274	-0.00079	1.147

https://doi.org/10.5194/tc-2020-53
Preprint. Discussion started: 17 March 2020

506	1.175	0.034	0.999	0.0276	-0.00080	1.150
507	1.186	0.035	0.999	0.0281	-0.00081	1.160
508	1.197	0.030	0.999	0.0287	-0.00083	1.172
509	1.204	0.034	0.999	0.0289	-0.00084	1.177
510	1.209	0.035	0.999	0.0292	-0.00085	1.182
511	1.223	0.036	0.999	0.0298	-0.00086	1.195
512	1.226	0.036	0.999	0.0299	-0.00087	1.197
513	1.235	0.032	0.999	0.0305	-0.00088	1.207
514	1.245	0.036	0.999	0.0310	-0.00090	1.217
515	1.255	0.036	0.999	0.0314	-0.00091	1.226
516	1.258	0.039	0.998	0.0316	-0.00092	1.229
517	1.264	0.030	0.999	0.0321	-0.00093	1.239
518	1.270	0.032	0.999	0.0323	-0.00094	1.243
519	1.286	0.038	0.999	0.0331	-0.00096	1.256
520	1.297	0.035	0.999	0.0336	-0.00097	1.266
521	1.304	0.034	0.999	0.0340	-0.00098	1.273
522	1.314	0.035	0.999	0.0345	-0.00100	1.283
523	1.327	0.036	0.999	0.0352	-0.00102	1.295
524	1.337	0.042	0.998	0.0357	-0.00103	1.304
525	1.346	0.036	0.999	0.0361	-0.00105	1.312
526	1.348	0.038	0.999	0.0363	-0.00105	1.314
527	1.366	0.034	0.999	0.0373	-0.00108	1.332
528	1.376	0.041	0.999	0.0379	-0.00110	1.342
529	1.383	0.041	0.999	0.0382	-0.00111	1.348
530	1.393	0.040	0.999	0.0388	-0.00112	1.358
531	1.402	0.040	0.999	0.0394	-0.00114	1.369
532	1.419	0.039	0.999	0.0402	-0.00117	1.382
533	1.428	0.037	0.999	0.0408	-0.00118	1.391
534	1.440	0.040	0.999	0.0414	-0.00120	1.402
535	1.453	0.039	0.999	0.0422	-0.00122	1.415
536	1.461	0.041	0.999	0.0426	-0.00124	1.422
537	1.475	0.038	0.999	0.0435	-0.00126	1.436
538	1.486	0.041	0.999	0.0441	-0.00128	1.446

https://doi.org/10.5194/tc-2020-53
Preprint. Discussion started: 17 March 2020


The Cryosphere Discussions
Open Access
EGU

539	1.501	0.041	0.999	0.0450	-0.00130	1.459
540	1.507	0.042	0.999	0.0454	-0.00131	1.466
541	1.519	0.040	0.999	0.0462	-0.00134	1.478
542	1.533	0.045	0.999	0.0470	-0.00136	1.491
543	1.545	0.044	0.999	0.0477	-0.00138	1.501
544	1.560	0.041	0.999	0.0486	-0.00141	1.516
545	1.576	0.043	0.999	0.0495	-0.00143	1.528
546	1.586	0.044	0.999	0.0502	-0.00146	1.540
547	1.600	0.044	0.999	0.0512	-0.00148	1.554
548	1.614	0.043	0.999	0.0520	-0.00151	1.567
549	1.623	0.046	0.999	0.0526	-0.00152	1.575
550	1.641	0.046	0.999	0.0537	-0.00156	1.591
551	1.649	0.049	0.999	0.0546	-0.00158	1.604
552	1.664	0.048	0.999	0.0554	-0.00161	1.615
553	1.679	0.047	0.999	0.0564	-0.00163	1.628
554	1.699	0.050	0.999	0.0576	-0.00167	1.645
555	1.709	0.051	0.999	0.0583	-0.00169	1.655
556	1.720	0.050	0.999	0.0591	-0.00171	1.667
557	1.742	0.049	0.999	0.0604	-0.00175	1.684
558	1.749	0.050	0.999	0.0611	-0.00177	1.693
559	1.763	0.053	0.999	0.0621	-0.00180	1.706
560	1.776	0.054	0.998	0.0629	-0.00182	1.717
561	1.793	0.055	0.998	0.0641	-0.00186	1.734
562	1.802	0.053	0.999	0.0649	-0.00188	1.743
563	1.816	0.053	0.999	0.0660	-0.00191	1.757
564	1.831	0.051	0.999	0.0670	-0.00194	1.770
565	1.850	0.054	0.999	0.0684	-0.00198	1.787
566	1.861	0.055	0.999	0.0691	-0.00200	1.796
567	1.874	0.053	0.999	0.0703	-0.00203	1.811
568	1.891	0.058	0.998	0.0715	-0.00207	1.827
569	1.904	0.055	0.999	0.0725	-0.00210	1.839
570	1.925	0.059	0.998	0.0740	-0.00214	1.857
571	1.934	0.061	0.998	0.0746	-0.00216	1.865

https://doi.org/10.5194/tc-2020-53
Preprint. Discussion started: 17 March 2020

572	1.958	0.058	0.999	0.0763	-0.00221	1.884
573	1.960	0.059	0.999	0.0769	-0.00223	1.892
574	1.981	0.060	0.998	0.0785	-0.00227	1.910
575	1.992	0.061	0.998	0.0793	-0.00230	1.920
576	2.013	0.062	0.998	0.0809	-0.00234	1.939
577	2.024	0.065	0.998	0.0817	-0.00237	1.948
578	2.042	0.065	0.998	0.0830	-0.00240	1.963
579	2.055	0.067	0.998	0.0848	-0.00246	1.983
580	2.068	0.068	0.998	0.0856	-0.00248	1.992
581	2.086	0.063	0.998	0.0869	-0.00252	2.007
582	2.106	0.063	0.999	0.0886	-0.00257	2.025
583	2.126	0.066	0.998	0.0900	-0.00261	2.041
584	2.140	0.069	0.998	0.0911	-0.00264	2.052
585	2.154	0.069	0.998	0.0928	-0.00269	2.071
586	2.175	0.066	0.998	0.0946	-0.00274	2.090
587	2.193	0.071	0.998	0.0961	-0.00278	2.106
588	2.208	0.070	0.998	0.0973	-0.00282	2.119
589	2.230	0.074	0.998	0.0991	-0.00287	2.137
590	2.252	0.077	0.998	0.1008	-0.00292	2.155
591	2.262	0.075	0.998	0.1026	-0.00297	2.173
592	2.286	0.077	0.998	0.1043	-0.00302	2.190
593	2.303	0.078	0.998	0.1061	-0.00307	2.208
594	2.322	0.075	0.998	0.1077	-0.00312	2.224
595	2.348	0.076	0.998	0.1101	-0.00319	2.247
596	2.366	0.078	0.998	0.1115	-0.00323	2.261
597	2.393	0.081	0.998	0.1143	-0.00331	2.288
598	2.403	0.078	0.998	0.1157	-0.00335	2.301
599	2.428	0.078	0.998	0.1179	-0.00341	2.322
600	2.451	0.076	0.998	0.1200	-0.00348	2.342
601	2.471	0.081	0.998	0.1219	-0.00353	2.359
602	2.485	0.077	0.998	0.1233	-0.00357	2.372
603	2.519	0.078	0.998	0.1264	-0.00366	2.400
604	2.538	0.082	0.998	0.1283	-0.00372	2.417

https://doi.org/10.5194/tc-2020-53
Preprint. Discussion started: 17 March 2020

605	2.549	0.080	0.998	0.1300	-0.00377	2.433
606	2.571	0.078	0.998	0.1322	-0.00383	2.452
607	2.595	0.081	0.998	0.1346	-0.00390	2.473
608	2.622	0.084	0.998	0.1372	-0.00398	2.496
609	2.649	0.082	0.998	0.1399	-0.00405	2.519
610	2.667	0.083	0.998	0.1417	-0.00410	2.534
611	2.695	0.087	0.998	0.1441	-0.00417	2.554
612	2.703	0.083	0.998	0.1465	-0.00424	2.575
613	2.735	0.086	0.998	0.1497	-0.00434	2.601
614	2.771	0.088	0.998	0.1534	-0.00444	2.631
615	2.789	0.087	0.998	0.1554	-0.00450	2.647
616	2.812	0.092	0.998	0.1579	-0.00457	2.667
617	2.841	0.087	0.998	0.1608	-0.00466	2.690
618	2.872	0.091	0.998	0.1646	-0.00477	2.721
619	2.878	0.092	0.998	0.1666	-0.00483	2.736
620	2.909	0.094	0.998	0.1702	-0.00493	2.764
621	2.939	0.093	0.998	0.1726	-0.00500	2.782
622	2.983	0.099	0.998	0.1778	-0.00515	2.821
623	2.998	0.097	0.998	0.1795	-0.00520	2.834
624	3.046	0.098	0.998	0.1850	-0.00536	2.875
625	3.066	0.099	0.998	0.1870	-0.00542	2.889
626	3.102	0.096	0.998	0.1913	-0.00554	2.920
627	3.105	0.097	0.998	0.1929	-0.00559	2.932
628	3.142	0.102	0.998	0.1986	-0.00575	2.972
629	3.173	0.102	0.998	0.2013	-0.00583	2.991
630	3.201	0.104	0.998	0.2048	-0.00593	3.015
631	3.243	0.105	0.998	0.2101	-0.00608	3.051
632	3.287	0.106	0.998	0.2154	-0.00624	3.088
633	3.291	0.108	0.998	0.2155	-0.00624	3.088
634	3.335	0.106	0.998	0.2217	-0.00642	3.129
635	3.365	0.110	0.998	0.2244	-0.00650	3.147
636	3.365	0.105	0.998	0.2271	-0.00658	3.165
637	3.405	0.111	0.998	0.2320	-0.00672	3.197

https://doi.org/10.5194/tc-2020-53
Preprint. Discussion started: 17 March 2020


The Cryosphere Discussions
Open Access
EGU

638	3.432	0.114	0.998	0.2356	-0.00682	3.220
639	3.457	0.109	0.998	0.2387	-0.00692	3.240
640	3.481	0.109	0.998	0.2422	-0.00701	3.261
641	3.551	0.113	0.998	0.2511	-0.00727	3.317
642	3.547	0.113	0.998	0.2519	-0.00730	3.322
643	3.585	0.113	0.998	0.2566	-0.00743	3.350
644	3.604	0.108	0.999	0.2595	-0.00752	3.368
645	3.624	0.117	0.998	0.2636	-0.00763	3.392
646	3.643	0.115	0.998	0.2652	-0.00768	3.402
647	3.697	0.121	0.998	0.2727	-0.00790	3.447
648	3.736	0.125	0.998	0.2787	-0.00807	3.482
649	3.746	0.120	0.998	0.2803	-0.00812	3.491
650	3.767	0.123	0.998	0.2833	-0.00821	3.508
651	3.797	0.121	0.998	0.2874	-0.00832	3.531
652	3.830	0.128	0.998	0.2916	-0.00845	3.555
653	3.865	0.129	0.998	0.2969	-0.00860	3.584
654	3.886	0.131	0.998	0.2996	-0.00868	3.600
655	3.939	0.138	0.998	0.3098	-0.00897	3.656
656	3.897	0.126	0.998	0.3046	-0.00882	3.627
657	3.908	0.117	0.999	0.3087	-0.00894	3.650
658	3.972	0.127	0.998	0.3148	-0.00912	3.683
659	4.001	0.129	0.998	0.3198	-0.00926	3.710
660	4.064	0.140	0.998	0.3298	-0.00955	3.763
661	4.027	0.128	0.998	0.3238	-0.00938	3.731
662	4.072	0.134	0.998	0.3309	-0.00958	3.768
663	4.092	0.132	0.998	0.3345	-0.00969	3.788
664	4.076	0.128	0.998	0.3331	-0.00965	3.780
665	4.163	0.140	0.998	0.3432	-0.00994	3.832
666	4.157	0.135	0.998	0.3437	-0.00996	3.835
667	4.123	0.128	0.998	0.3423	-0.00992	3.828
668	4.147	0.129	0.998	0.3446	-0.00998	3.839
669	4.181	0.131	0.998	0.3503	-0.01015	3.869
670	4.229	0.142	0.998	0.3565	-0.01033	3.900

https://doi.org/10.5194/tc-2020-53
Preprint. Discussion started: 17 March 2020

671	4.177	0.122	0.999	0.3494	-0.01012	3.864
672	4.257	0.139	0.998	0.3620	-0.01049	3.927
673	4.240	0.130	0.998	0.3591	-0.01040	3.913
674	4.293	0.138	0.998	0.3679	-0.01066	3.956
675	4.345	0.148	0.998	0.3749	-0.01086	3.991
676	4.338	0.140	0.998	0.3740	-0.01083	3.986
677	4.353	0.141	0.998	0.3756	-0.01088	3.994
678	4.364	0.137	0.998	0.3828	-0.01109	4.029
679	4.340	0.135	0.998	0.3798	-0.01100	4.014
680	4.436	0.147	0.998	0.3914	-0.01134	4.070
681	4.391	0.140	0.998	0.3884	-0.01125	4.056
682	4.366	0.132	0.998	0.3815	-0.01105	4.023
683	4.540	0.159	0.998	0.4107	-0.01190	4.160
684	4.454	0.143	0.998	0.3986	-0.01155	4.104
685	4.559	0.151	0.998	0.4167	-0.01207	4.188
686	4.599	0.160	0.998	0.4212	-0.01220	4.208
687	4.475	0.137	0.998	0.4008	-0.01161	4.114
688	4.596	0.148	0.998	0.4216	-0.01221	4.210
689	4.626	0.146	0.998	0.4278	-0.01239	4.238
690	4.650	0.151	0.998	0.4344	-0.01258	4.268
691	4.729	0.165	0.998	0.4412	-0.01278	4.297
692	4.611	0.136	0.999	0.4306	-0.01247	4.250
693	4.790	0.168	0.998	0.4542	-0.01316	4.355
694	4.558	0.123	0.999	0.4288	-0.01242	4.241
695	4.832	0.162	0.998	0.4683	-0.01357	4.415
696	4.837	0.149	0.998	0.4714	-0.01366	4.428
697	4.850	0.156	0.998	0.4791	-0.01388	4.461
698	4.922	0.157	0.998	0.4951	-0.01434	4.527
699	5.060	0.182	0.998	0.4996	-0.01447	4.545
700	5.021	0.159	0.998	0.5027	-0.01456	4.559